



# A new bootstrap technique to quantify uncertainty in estimates of ground surface temperature and ground heat flux histories from geothermal data

Francisco José Cuesta-Valero<sup>1,2</sup>, Hugo Beltrami<sup>3</sup>, Stephan Gruber<sup>4</sup>, Almudena García-García<sup>1,2</sup>, and J. Fidel González-Rouco<sup>5</sup>

<sup>1</sup>Department of Remote Sensing, Helmholtz Centre for Environmental Research (UFZ), Permoserstraße 15, Leipzig, 04318, Saxony, Germany

<sup>2</sup>Remote Sensing Centre for Earth System Research, Leipzig University, 04103, Leipzig, Germany

<sup>3</sup>Climate & Atmospheric Sciences Institute, St. Francis Xavier University, 5009 Chapel Square, Antigonish, B2G 2W5, NS, Canada

<sup>4</sup>Department of Geography and Environmental Studies, Carleton University, 1125 Colonel By Dr, Ottawa, K1S 5B6, ON, Canada

<sup>5</sup>Instituto de Geociencias, Consejo Superior de Investigaciones Científicas – Universidad Complutense de Madrid, Madrid, Spain

**Correspondence:** Francisco José Cuesta-Valero (francisco-jose.cuesta-valero@ufz.de)

Received: 11 July 2022 – Discussion started: 19 July 2022

Revised: 6 October 2022 – Accepted: 11 October 2022 – Published: 28 October 2022

**Abstract.** Estimates of the past thermal state of the land surface are crucial to assess the magnitude of current anthropogenic climate change as well as to assess the ability of Earth System Models (ESMs) to forecast the evolution of the climate near the ground, which is not included in standard meteorological records. Subsurface temperature reacts to long-term changes in surface energy balance – from decadal to millennial time scales – thus constituting an important record of the dynamics of the climate system that contributes, with low-frequency information, to proxy-based paleoclimatic reconstructions. Broadly used techniques to retrieve past temperature and heat flux histories from subsurface temperature profiles based on a singular value decomposition (SVD) algorithm were able to provide robust global estimates for the last millennium, but the approaches used to derive the corresponding 95 % confidence interval were wrong from a statistical point of view in addition to being difficult to interpret. To alleviate the lack of a meaningful framework for estimating uncertainties in past temperature and heat flux histories at regional and global scales, we combine a new bootstrapping sampling strategy with the broadly used SVD algorithm and assess its performance against the

original SVD technique and another technique based on generating perturbed parameter ensembles of inversions. The new bootstrap approach is able to reproduce the prescribed surface temperature series used to derive an artificial profile. Bootstrap results are also in agreement with the global mean surface temperature history and the global mean heat flux history retrieved in previous studies. Furthermore, the new bootstrap technique provides a meaningful uncertainty range for the inversion of large sets of subsurface temperature profiles. We suggest the use of this new approach particularly for aggregating results from a number of individual profiles, and to this end, we release the programs used to derive all inversions in this study as a suite of codes labeled CIBOR v1: Codes for Inverting BORholes, version 1.

## 1 Introduction

Anthropogenic activities have contributed to a sustained increase in the Earth's energy imbalance at the top of the atmosphere (Hansen et al., 2011; Stephens et al., 2012; Johnson et al., 2016; Marti et al., 2022), inducing a radiative re-

sponse from the climate system (Donohoe et al., 2014). As part of this response, energy exchanges among the ocean, the cryosphere, the continental land masses, and the atmosphere have been altered, leading to an increase in the heat stored in these components of the Earth system (Hansen et al., 2011; von Schuckmann et al., 2020). The ocean accounts for around 89 % of the additional heat storage, with continental landmasses being the second largest component, storing 6 % of the total heat, followed by the cryosphere (4 %) and the atmosphere (1 %). Monitoring the evolution of the Earth's heat inventory is of critical importance to understand the state of the climate system, the magnitude of climate change, and future societal and ecosystem risks. Changes in heat storage within each component affect the dynamics of important phenomena – for example, heat uptake by the cryosphere contributes to sea level rise (Oppenheimer et al., 2019), heat gain by the atmosphere affect the development of extreme precipitation events (Pendergrass and Hartmann, 2014), and heat gain by the continental subsurface can increase the release of greenhouse gases from northern soils (Hicks Pries et al., 2017; McGuire et al., 2018).

Most global estimates of continental heat storage have been inferred from subsurface temperature profiles (STPs) (Beltrami et al., 2002; Beltrami, 2002; von Schuckmann et al., 2020; Cuesta-Valero et al., 2021c), which allow for the estimation of past ground surface temperature and ground heat flux changes at decadal to centennial time scales (e.g., Shen et al., 1992; Beltrami et al., 2002; Beltrami, 2002; Hopcroft et al., 2007; Demezhko and Gornostaeva, 2015a; Kukkonen et al., 2020). These long-term estimates of surface temperature and ground heat flux changes have also been used to evaluate the ability of general circulation models (GCMs) to reproduce past changes in the conditions of the shallow continental subsurface, which has increased our knowledge of the Earth system as well as our confidence in future projections (González-Rouco et al., 2006; González-Rouco et al., 2009; García-García et al., 2016; Cuesta-Valero et al., 2019; Melo-Aguilar et al., 2020). Furthermore, ground surface temperature and heat flux reconstructions from subsurface temperature data have been essential for informing the development of land surface model components, improving the representation of heat transfer through the continental subsurface in climate simulations (Alexeev et al., 2007; Nicolsky et al., 2007; Stevens et al., 2007, 2008; MacDougall et al., 2010; Cuesta-Valero et al., 2016; Hermoso de Mendoza et al., 2020; Cuesta-Valero et al., 2021b; González-Rouco et al., 2021).

Several techniques exist to retrieve the evolution of ground surface temperature changes from STPs, all yielding similar results (Beltrami and Mareschal, 1992; Shen et al., 1992; Hartmann and Rath, 2005; Hopcroft et al., 2007; Cuesta-Valero et al., 2021c). These techniques solve the inversion problem – that is, estimating the changes in surface temperature that generated the observed profile – with two main strategies to retrieve STP inversions: Bayesian

methods (Shen et al., 1992; Woodbury and Ferguson, 2006; Hopcroft et al., 2007, 2009) and methods based on a singular value decomposition (SVD) algorithm (Beltrami et al., 1992; Beltrami and Mareschal, 1992; Clauser and Mareschal, 1995; Hartmann and Rath, 2005; Jaume-Santero et al., 2016; Cuesta-Valero et al., 2021c). Nevertheless, several sources of uncertainty arise in the inversion process, the most important being the unknown thermal properties at most sites, the determination of the quasi-equilibrium temperature profile at each site, and the value of several parameters in the inversion framework, such as the number and length of the time steps for modeling the retrieved surface temperature series and the number of eigenvalues retained in the SVD algorithm to obtain stable solutions. Bayesian frameworks allow one to easily include different sources of uncertainty in the inversions, while the methods based on applying the SVD algorithm are less flexible, requiring the development of additional sampling strategies to include the different uncertainties in the inversions.

A broadly used method to include the uncertainty due to the unknown quasi-equilibrium temperature profile at each site in SVD inversions consists of performing a linear regression analysis of the deepest part of the observed profile, then providing a best estimate of the quasi-equilibrium profile and using the error in the regression coefficients to generate two extremal profiles that constitute the upper and lower limit of the uncertainty range (e.g., Beltrami et al., 2015a, b). The anomaly profiles obtained by subtracting these three profiles from the measured STP are then inverted, providing a best estimate of the past ground surface temperature history and an uncertainty range given by the inversion of the two extremal profiles. Repeating the SVD inversion using different time step lengths to characterize the surface temperature series and retaining a different number of eigenvalues in the solution allow us to assess the effect of each parameter in the retrieved inversion (e.g., González-Rouco et al., 2009). Nevertheless, including the uncertainty due to unknown thermal properties in the ground into SVD inversions required the development of a different approach. This new approach was labeled perturbed parameter inversion (PPI), because it was based on estimating a large ensemble of SVD inversions by changing the value of the inversion parameters for each iteration, including the value of thermal properties (Cuesta-Valero et al., 2021c). After generating the ensemble, the 2.5th, 50th, and 97.5th percentiles of all solutions are computed in order to obtain a best estimate and a 95 % confidence interval. Thereby, the PPI approach is a generalization of the SVD algorithm, including the uncertainty due to all important factors described above in the inversions of individual profiles.

Estimates of ground heat flux histories have been retrieved from STPs using two main methods: inversion of subsurface heat flux profiles and from ground surface temperature histories. Subsurface heat flux profiles can be estimated directly from measured STPs using the Fourier equation, and due to the nature of heat diffusion through the ground,

these heat flux profiles can be inverted following the same SVD approach used to invert subsurface temperature profiles (Beltrami, 2001; Turcotte and Schubert, 2002; Cuesta-Valero et al., 2021c). Nevertheless, subsurface heat flux profiles are noisier than STPs; thus, the uncertainty in the retrieved ground heat flux histories is large. The other approach consists of applying the solution of the heat diffusion equation obtained in Wang and Bras (1999) to the ground surface temperature history estimated by inverting the corresponding STP, reducing the noise in the retrieved ground heat flux history (Beltrami et al., 2002). Both techniques have shown similar results in the past (Cuesta-Valero et al., 2021c).

Although both SVD and PPI approaches are able to retrieve ground surface temperature and ground heat flux histories from individual STPs, these techniques do not include a meaningful, interpretable framework for aggregating inversions from sets of different profiles. An approach used in the past to obtain regional and global estimates consisted of simultaneously inverting all logs in a given dataset, retrieving a unique ground surface temperature history representing the zonal average (Beltrami, 2002). Nevertheless, this approach is better used with profiles measured at similar dates, because it considers only one surface temperature series, and thus, it does not include the effect of the different logging years of each STP on the solution. Alternatively, regional and global averages can be estimated as the mean of ground surface temperature histories (Cuesta-Valero et al., 2021c). However, the most important caveat in the SVD and PPI methods for aggregating individual inversions consists of determining the confidence interval for the averaged temperature and heat flux histories. The uncertainty range for the SVD case is estimated as the mean of the solutions from the extremal anomaly profiles retrieved for each measured STP and as the mean of the 2.5th and 97.5th percentiles from each profile in the case of PPI solutions. These methodologies were developed as a markedly conservative case, trying to include the true uncertainty of the mean in the estimates, even if overestimating the reported 95 % confidence interval. Nevertheless, those methodologies are wrong from a statistical point of view, and a new method based on solid statistical principles needs to be developed to provide correct, interpretable confidence intervals for the averaged histories from individual STP inversions.

Here, we introduce a new statistical framework to improve estimates of uncertainty in ground surface temperature and ground heat flux histories from SVD inversions. This new method is based on a bootstrap technique to sample the plausible values of poorly known inversion parameters, together with a broadly used SVD algorithm, that can be applied to any number of profiles. Results from this new approach – hereinafter referred to as bootstrap inversions – are compared against those from the original SVD method and the PPI approach. An artificial temperature profile and real STP measurements from the Xibalbá dataset (Cuesta-Valero et al., 2021a) are inverted using these techniques. Using an artificial

profile generated from a known boundary condition allows for an evaluation of the performance of each method and the choice of parameters against a known surface signal before estimating global surface temperature histories and global ground heat flux histories from a large dataset of subsurface temperature profiles. These experiments allow for the identification of shortcomings in the uncertainty ranges derived from the typical SVD and PPI techniques, particularly when aggregating a large number of profiles. Our results reinforce the role of the STP inversions as indicators of the long-term evolution of surface conditions.

## 2 Data

### 2.1 Proxy-based temperatures

Global temperature reconstructions from those in Fig. 1 of the Summary for Policymakers of the sixth Assessment Report of the Intergovernmental Panel on Climate Change (IPCC) are used here for comparison purposes and to generate synthetic data to test the inversion methods (IPCC, 2021). These reconstructions are based on multi-proxy systems, such as corals and tree rings, and were estimated by the 2k Network of the Past Global Changes organization (PAGES2k) (Neukom et al., 2019; PAGES2k Consortium, 2022). The global mean temperature anomaly is provided as a smoothed temporal series using a 10-year window; thus, data are available from year 5 to 1995 of the Common Era (CE).

PAGES2k reconstructions combine land and marine proxies to produce global mean temperatures, which we transform into global land temperatures. To this end, we apply the ratio between land and ocean temperature changes estimated in Harrison et al. (2015) based on an ensemble of global climate simulations. This multimodel ensemble includes different forcing scenarios at several time scales, resulting in land surface temperature changes being  $\sim 2.36$  times larger than sea surface temperature changes. Therefore, the PAGES2k global temperature anomaly can be scaled to land temperature changes multiplying by  $\sim 1.38$ . The same procedure is applied to the provided uncertainty range, as prescribed by the error propagation theory. The resulting temperature anomaly after the scaling is modified to have 1300–1700 CE as period of reference, the same as the inversions of subsurface temperature profiles (see below). The land temperature anomaly from the PAGES2k global temperature anomaly, labeled PAGES2k-Land temperature hereinafter, is used as the upper boundary condition to derive an artificial subsurface temperature profile designed to test the performance of the different methods considered here. Additionally, inversions of the Xibalbá database are also compared with these PAGES2k-Land temperatures.

## 2.2 Xibalbá subsurface temperature profiles

Subsurface temperature profiles from the Xibalbá dataset (Cuesta-Valero et al., 2021a, c) are inverted to estimate global mean ground surface temperature histories. Xibalbá profiles were assembled using measurements from several sources, including the National Oceanic and Atmospheric Administration (NOAA) server (NOAA, 2019) and several publications (Jaume-Santero et al., 2016; Suman et al., 2017; Pickler et al., 2018). Each log was screened to ensure that the profiles did not contain obvious non-climatic signals due to water flow or other factors. All logs were truncated to contain depths between 15 and 300 m to ensure that all profiles produced inversions relative to the same temporal period (González-Rouco et al., 2009; Beltrami et al., 2011, 2015a; Cuesta-Valero et al., 2019; Melo-Aguilar et al., 2020).

The dataset includes 1079 STPs distributed around the world, although with a lack of measurements in South America, most of Africa, the Middle East, and southeastern Asia (see Fig. 1 in Cuesta-Valero et al., 2021c). Furthermore, all STPs were measured at different dates, with the majority of profiles obtained before the year 2000 CE. Hence, we aggregate the inversions of these logs, respecting their different logging years, thus obtaining results with a different number of inversions per year and focused on the period before the year 2000 CE.

An important caveat of the Xibalbá dataset is the lack of measurements of thermal properties at the location of the profiles. Most measurements of temperature profiles provide no thermal property data, thus requiring assumptions about thermal diffusivity and conductivity values in order to perform the analysis. The continental subsurface is typically considered as an homogeneous medium because of this limitation, which is supported by the few profiles including measurements of thermal properties. These measurements show that thermal properties vary by a relatively small amount around a mean value with depth (e.g., the Neil Well in the Arctic (Beltrami and Taylor, 1995)). Additionally, the screening process for all individual logs (see above) helps to exclude profiles at locations with marked changes in thermal properties, since these changes would be reflected in the temperature records as non-climatic signals.

## 3 Methods

The new CIBOR v1 (Codes for Inverting BORholes, version 1) is a collection of scripts for performing SVD inversions of subsurface temperature profiles, including three different strategies to aggregate results from any number of individual profiles, which is fundamental to deriving regional and global averages of past ground surface temperature and ground heat flux histories. This section explains the general physical and statistical principles to perform SVD inversions of subsurface temperature profiles and to estimate the uncertainties in-

involved in the process, as included in the CIBOR v1 scripts. For information about the accessibility of the codes, please check the Code availability statement at the end of this article.

### 3.1 Subsurface temperature profiles

Ground temperature changes with depth as a response to the surface energy balance variations and the heat flow from the Earth's interior, constant at time scales of millions of years (Jaupard and Mareschal, 2010). These variations in the surface energy balance are propagated through the ground following the one-dimensional heat diffusion equation, altering the quasi-equilibrium temperature profile resulting from the long-term surface temperature ( $T_0$ ) and geothermal gradient ( $\Gamma_0$ ). Assuming constant thermal properties through the ground column, a subsurface temperature profile can be described as (Carslaw and Jaeger, 1959)

$$T(z, t) = T_0 + \Gamma_0 \cdot z + T_t(z), \quad (1)$$

where  $z$  is depth, the term  $T_0 + \Gamma_0 \cdot z$  constitutes the quasi-equilibrium temperature profile, and the term  $T_t(z)$  represents the signature of recent changes in the surface energy balance.

The quasi-equilibrium temperature profile represents the long-term mean thermal state of the subsurface without changes in the surface energy balance and in the geothermal flux from the Earth's interior – that is, the profile resulting from a constant surface temperature and a constant geothermal gradient. Changes in the surface energy balance propagate through the ground by conduction and are recorded as alterations of this quasi-equilibrium profile. The propagation of a perturbation modeled as a step change in surface temperature ( $\Delta T$ ) at a certain time  $t$  in the past through a homogeneous medium can be described as (Carslaw and Jaeger, 1959)

$$T(z) = \Delta T \cdot \operatorname{erfc}\left(\frac{z}{2\sqrt{\kappa \cdot t}}\right), \quad (2)$$

where  $\operatorname{erfc}$  is the complementary error function,  $\kappa$  is the thermal diffusivity of the medium, and  $z$  is depth. Therefore, the final anomaly profile caused by the propagation of a series of step changes in surface temperatures ( $\Delta T_i$ ) through the ground can be expressed as

$$T_t(z) = \sum_{i=1}^N \Delta T_i \cdot \left[ \operatorname{erfc}\left(\frac{z}{2\sqrt{\kappa \cdot t_i}}\right) - \operatorname{erfc}\left(\frac{z}{2\sqrt{\kappa \cdot t_{i-1}}}\right) \right], \quad (3)$$

which represents the depth-varying temperature term in Eq. (1).  $T_t(z)$  is the solution of the forward problem – that is, for a given surface temperature time series. Equation (3) provides the final perturbation of the subsurface profile in response to changes in the upper boundary condition. Therefore, Eq. (3) constitutes a one-dimensional forward model of heat diffusion through the ground.

### 3.2 Artificial profile

An artificial STP is generated using the PAGES2k-Land temperature as the upper boundary condition for a purely conductive, homogeneous, half-space forward model (see Eq. 3). From the PAGES2k-Land temperatures, this forward model generates a temperature profile that contains the changes in subsurface temperatures as a response to the prescribed changes in surface temperatures with time. A quasi-equilibrium temperature profile consisting of a long-term surface temperature of 8 °C and a long-term geothermal gradient of 20 °C km<sup>-1</sup> is added to the profile in addition to Gaussian noise with zero mean and a standard deviation of 0.02 °C to account for measurement uncertainties in real profiles (Beltrami et al., 2015a). Ground surface temperature histories are estimated from the inversion of the resulting artificial profile (Fig. 1) using the three techniques detailed below. These temperature histories are then evaluated against the original PAGES2k-Land temperatures that were used as boundary conditions to generate the synthetic data to evaluate the performance of each technique.

### 3.3 SVD inversions

The inversion problem for STPs consists of estimating the magnitude of the past changes in surface temperature that gave rise to the observed variation of temperature with depth. Such changes in surface temperature are typically modeled as a series of step changes whose magnitude is determined by the inversion technique, with the length of the time step set as a parameter. One of the standard methodologies to perform these inversions is based on solving a system of equations given by the observed profile and the combination of Eqs. (1) and (3) (Vasseur et al., 1983; Beltrami et al., 1992; Shen et al., 1992; Hartmann and Rath, 2005). This approach uses a singular value decomposition (SVD) algorithm to solve this system, and it is known as the SVD inversion method (Fig. 1). The system considered in this inversion method can be expressed as

$$T_{\text{obs}} = \mathbf{M}T_{\text{model}}, \tag{4}$$

where  $T_{\text{obs}}$  is the anomaly temperature profile,  $T_{\text{model}}$  is a vector containing the step change model of the surface temperature to be determined, and  $\mathbf{M}$  is the matrix containing the coefficients given by

$$M_{i,j} = \text{erfc}\left(\frac{z_i}{2\sqrt{\kappa t_j}}\right) - \text{erfc}\left(\frac{z_i}{2\sqrt{\kappa t_{j-1}}}\right). \tag{5}$$

This system of equations, nevertheless, is overdetermined. This means that there are more equations in the system than parameters to be determined; thus, the solution is non-unique. A singular value decomposition (SVD) algorithm (Lanczos, 1961) has been extensively used to solve these overdetermined systems (e.g., Mareschal and Beltrami,

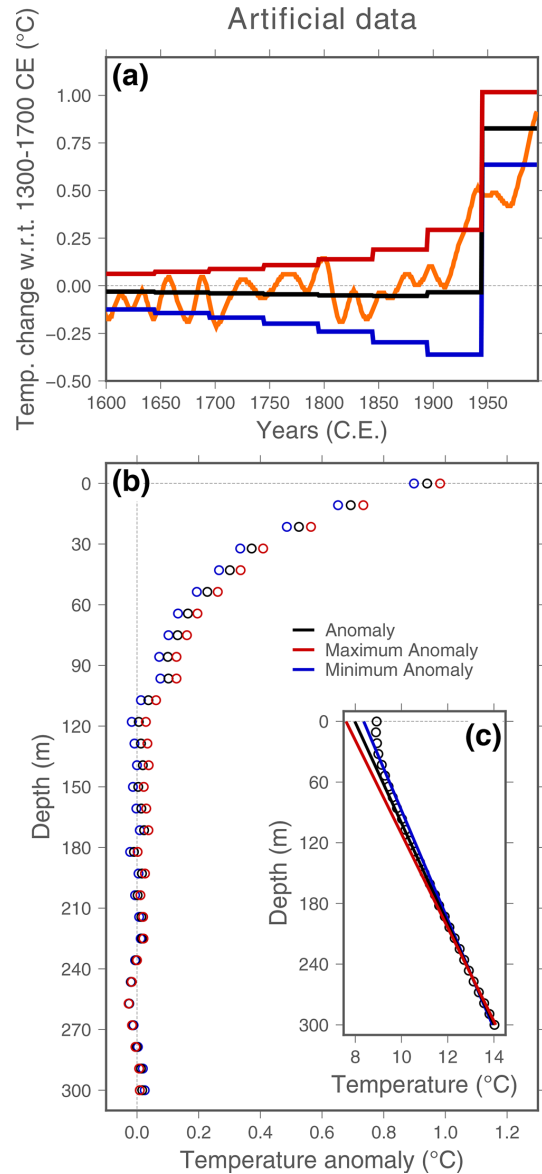


**Figure 1.** (a) Surface signal (orange line) and corresponding anomaly (b) and original (c) profiles for the artificial case. The surface signal corresponds to the PAGES2k-Land temperatures described in the Data section. The subsurface temperature profiles result from the propagation of the surface signal through the ground using a purely conductive forward model (see Methods section), considering a quasi-equilibrium profile given by a long-term surface temperature of  $T_0 = 8\text{ °C}$  and a geothermal gradient of  $\Gamma = 0.02\text{ °C m}^{-1}$ . Gaussian noise with  $\mu = 0.0\text{ °C}$  and  $\sigma = 0.02\text{ °C}$  is added to simulate measurement error. The extremal profiles (red and blue data) are estimated from a linear regression analysis of the deeper 100 m of the profile. The intercept of the extremal profiles in (c) has been modified for clarity. Temperature reconstructions from SVD inversions of each anomaly profile in (b) are shown in (a).

1992; Clauser and Mareschal, 1995; Jaume-Santero et al., 2016). The SVD algorithm is based on decomposing the matrix of coefficients  $\mathbf{M}$  into two orthogonal matrices ( $\mathbf{U}$  and  $\mathbf{V}$ ) and a rectangular matrix ( $\mathbf{S}$ ) containing the eigenvalues in the diagonal:

$$\mathbf{M} = \mathbf{USV}^T. \quad (6)$$

Thereby, the solution of the system can be found as

$$\mathbf{T}_{\text{model}} = \mathbf{VS}^{-1}\mathbf{U}^T \mathbf{T}_{\text{obs}}. \quad (7)$$

Finally, small eigenvalues are removed from  $\mathbf{S}^{-1}$  in order to stabilize the solution, though this is at the cost of losing temporal resolution in the model. The final number of eigenvalues used to retrieve the solution is an important parameter, typically retaining two or three eigenvalues. More details about SVD inversions can be found in the literature (Mareschal and Beltrami, 1992; Clauser and Mareschal, 1995; Beltrami, 2001; González-Rouco et al., 2009; Cuesta-Valero et al., 2021c).

The SVD inversion (Fig. 2) is applied to the anomaly profiles – that is, the resulting perturbation profiles after removing the quasi-equilibrium profile from the measured log (Fig. 1b, c). The quasi-equilibrium profile – in other words the term  $T_0 + \Gamma_0 \cdot z$  in Eq. (1) – is estimated using a linear regression analysis of the deepest 100 m of the corresponding profile, which is the part of the measured profile not affected by recent changes in surface conditions. The errors in the estimates of the long-term surface temperature ( $T_0$ ) and the geothermal gradient ( $\Gamma_0$ ) have been typically included in the analysis by inverting three anomaly profiles: the anomaly profile resulting from subtracting the best estimate of  $T_0$  and  $\Gamma_0$  from the measured profile (black dots in Fig. 1b), and two extremal profiles resulting from subtracting the quasi-equilibrium profiles determined by the errors in  $T_0$  and  $\Gamma_0$  (red and blue dots in Fig. 1b). These extremal profiles are derived by subtracting and adding the corresponding two sigma values to the best estimate of  $T_0$  and  $\Gamma_0$ . The inversions of the extremal anomaly profiles constitute the upper and lower boundaries of the uncertainty range (Beltrami et al., 2015a, b) in the retrieved ground surface temperature history of the corresponding log (red and blue lines in Fig. 1a).

Ground heat flux histories for each STP are estimated from ground surface temperature histories (see Sect. 3.6). Concretely, a flux history is estimated from each temperature history retrieved from each STP – that is, from the best estimate and the inversion of the two extremal anomaly profiles. Flux histories can also be retrieved from flux profiles, which can be estimated from the measured STPs by applying the Fourier equation (Beltrami, 2001; Cuesta-Valero et al., 2021c). Inversions of flux profiles are, nevertheless, noisier than inversions of temperature profiles; thus, we decided to derive heat flux histories from temperature histories in this analysis.

Please note that the method described in this section is applied to individual STPs – see Sect. 3.7 for a description of the approach used to obtain results from a set of profiles.

### 3.4 Perturbed parameter inversions

Inverting the extremal anomaly profiles obtained from the errors in estimating the long-term mean surface temperature and mean geothermal gradient allows one to account for the uncertainty in the determination of the quasi-equilibrium temperature profile in the SVD approach described above. Nevertheless, the SVD approach is not able to include the uncertainty due to the unknown thermal properties at each site. Hence, a more comprehensive way to estimate uncertainties in STP inversions was developed in Cuesta-Valero et al. (2021c). This approach, called perturbed parameter inversion (PPI), consists of generating a large ensemble of SVD inversions from each subsurface temperature profile by varying the values of the inversion parameters: time step of the surface signal, thermal diffusivity and conductivity, and the number of eigenvalues retained in Eq. (7) (Fig. 2). This process is repeated for the three anomaly profiles retrieved to characterize the uncertainty in the determination of the quasi-equilibrium temperature profile (see SVD technique above). We perturb only the parameters related to thermal properties and the quasi-equilibrium temperature profile in this study, as these are the most important sources of uncertainty (Cuesta-Valero et al., 2021c). That is, we generate an ensemble of inversions using the three anomaly profiles obtained from the best estimate and two sigma values of the intercept ( $T_0$ ) and slope ( $\Gamma_0$ ) determined from the linear regression of the deepest part of the profile, and considering a different thermal diffusivity for each inversion ( $N_{\text{Diffusivity}}$  in Fig. 2). Thereby, the ensemble contains  $3 \times N_{\text{Diffusivity}}$  elements. The 2.5th, 50th, and 97.5th percentiles of all retrieved temperature histories are then estimated in order to provide a best estimate (the median) and a 95 % confidence interval for the ground surface temperature history of each profile.

The PPI method described in Cuesta-Valero et al. (2021c) removed highly unlikely individual ground surface temperature histories from the final ensemble. However, here, we consider all possible histories in order to explore the full range of variability in the inversions, including unlikely cases. For the same reason, forward models of individual histories are not compared with the anomaly profiles, and thus, each history is weighted equal in the estimated percentiles, in contrast to the approach in Cuesta-Valero et al. (2021c). Thereby, the full effect of the unknown thermal properties in the estimated uncertainty can be assessed by comparing PPI solutions with SVD inversions, since the only difference between these two techniques is the use of a range of diffusivities in the PPI method.

Ground heat flux histories for each STP are estimated from ground surface temperature histories (see Sect. 3.6), similarly to the SVD case but with some differences. The PPI method

### Inversion Algorithms

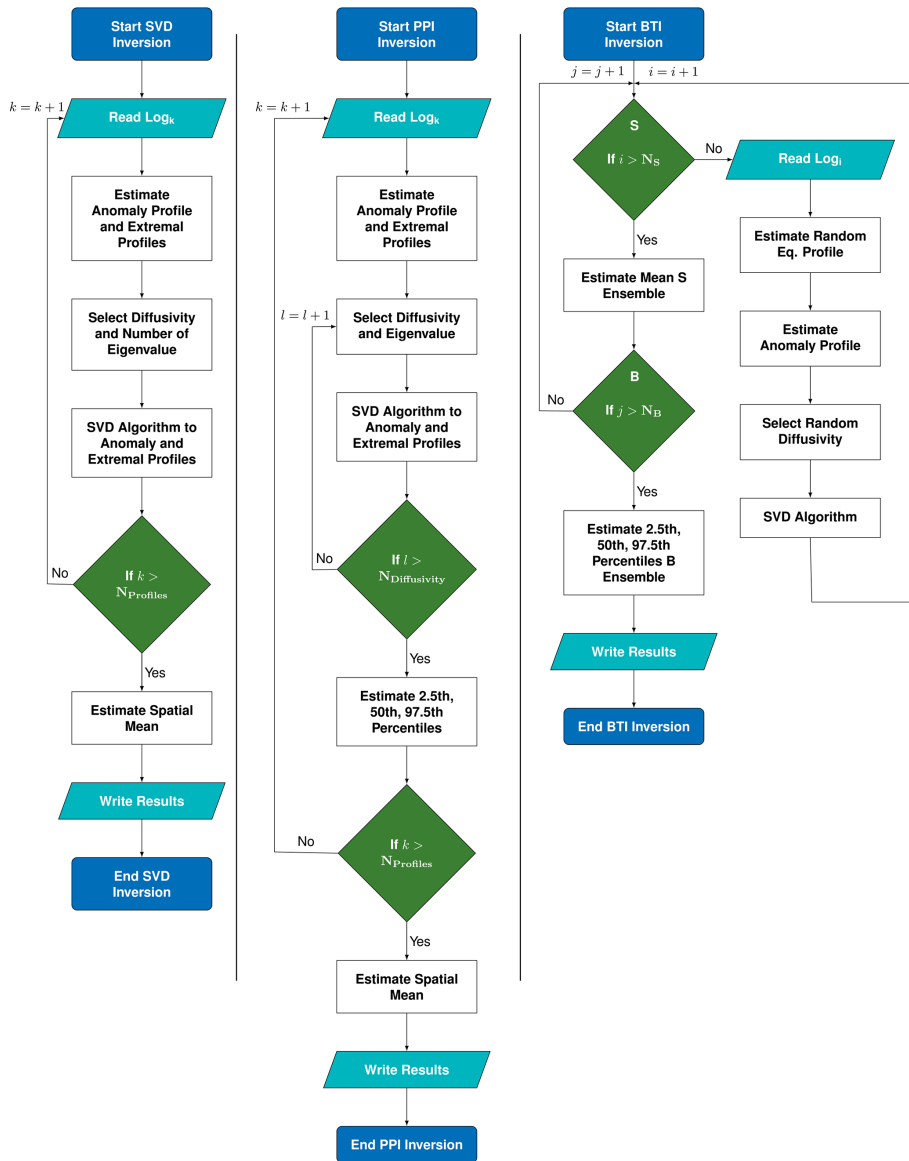


**Figure 2.** Flowchart diagram of the three methods used here to retrieve STP inversions: SVD (left), PPI (center), and BTI (right). All three methods are based on SVD inversions, but consider different approaches to estimate uncertainties. SVD and PPI methods invert three anomaly profiles from each log: the anomaly estimated from the quasi-equilibrium temperature profile and two extremal anomaly profiles estimated using the error in the determination of the quasi-equilibrium temperature profile, which provide the best estimate and the uncertainty of the results (see Fig. 1). The PPI technique also considers a range of possible thermal properties and a range of eigenvalues to retrieve the inversions. The BTI method considers a range of possible thermal properties and different quasi-equilibrium temperature profiles, but it aggregates solutions that consider different values of the parameters (and several logs if applicable) by following a bootstrap sampling strategy, while the SVD and PPI techniques just average the inversions of the three anomaly profiles. See Methods section for more details.

retrieves an ensemble of temperature histories for each STP. We estimate another ensemble containing flux histories using each of the temperature histories in the PPI ensemble, obtaining the 2.5th, 50th, and 97.5th percentiles that constitute the best estimate and uncertainty range for the ground heat flux history of the corresponding profile.

Note that this method is applied to individual STPs – see Sect. 3.7 for a description of the approach used to obtain results from a set of profiles.

### 3.5 Bootstrap sampling strategy

As explained in the Introduction, the SVD and PPI techniques do not provide a correct statistical framework to estimate the uncertainty resulting from aggregating inversions from several STPs. In order to overcome this problem, we have developed a new method to retrieve ground surface temperature histories combining the SVD algorithm described in Sect. 3.3 and a bootstrapping sampling strategy that provides a meaningful statistical method to estimate uncertainty ranges for aggregations of any number of individual profiles (Efron, 1987; DiCiccio and Efron, 1996; Davison and Hinkley, 1997).

Bootstrap Inversions (BTIs) are based on generating two ensembles – named Sampling and Bootstrapping ensembles (S and B ensembles in Fig. 2) – constituted by inversions performed using the SVD algorithm. The Sampling ensemble consists of one SVD inversion per subsurface temperature profile in the considered population, with inversion parameters randomly selected from a range of possibilities (e.g., the value for thermal diffusivity – see below). One thousand different Sampling ensembles are created, with the mean ground surface temperature history of each Sampling ensemble constituting an element of the Bootstrapping ensemble (Fig. 2). That is, the Bootstrapping ensemble includes one mean history per Sampling ensemble created. The median of the resulting Bootstrapping ensemble constitutes the best estimate for the mean ground surface temperature history of the considered population of logs, with the 95 % confidence interval given by the 2.5th and 97.5th percentiles of the Bootstrapping ensemble (Efron, 1987; DiCiccio and Efron, 1996; Davison and Hinkley, 1997). Here, we create 1000 different Sampling ensembles in each BTI inversion; thus, the Bootstrapping ensemble includes 1000 averaged histories. Larger sizes for the Bootstrapping ensemble can be considered, but the results are approximately the same (see analysis below).

There are four parameters used to obtain surface temperature histories in the Sampling ensemble described above: the prescribed quasi-equilibrium temperature profile, the assumed thermal properties of the ground, the length of the prescribed step changes to model the retrieved surface temperature, and the number of eigenvalues retained in the solution. However, the largest sources of uncertainty are the determination of the quasi-equilibrium profile (i.e., the errors in  $T_0$  and  $\Gamma_0$ ) and the unknown thermal diffusivity and conductivity of the subsurface (Table 1). For bootstrap inversions, all possible values for each parameter are equally probable, except for the quasi-equilibrium temperature profile. In this case, the long-term surface temperature and geothermal gradient are given by a Gaussian distribution, with mean and standard deviation corresponding to the best estimate and error of  $T_0$  and  $\Gamma_0$ , which are retrieved from the linear regression analysis of the deepest part of each profile.

Similarly to the SVD and PPI cases, ground heat flux histories are derived from ground surface temperature histories

for each STP. In this case, each temperature history considered in the Sampling ensemble is used to estimate a flux history, which is then averaged to obtain a mean ground heat flux history. The process is repeated 1000 times, as in the case of temperature histories, to generate a Bootstrapping ensemble containing mean flux histories, from which the 2.5th, 50th, and 97.5th percentiles are computed.

### 3.6 Ground heat flux histories

Ground heat flux histories are estimated using the method developed in Wang and Bras (1999) by using a half-order derivative approach to estimate ground heat flux from soil temperatures in a homogeneous medium. Since SVD inversions also assume a homogeneous subsurface, this method can be applied to the retrieved ground surface temperature histories to obtain ground heat flux histories (Beltrami et al., 2002; Cuesta-Valero et al., 2021c, among others). Given a temperature history with equidistant time steps ( $t_N$ ), the corresponding heat flux history is estimated as

$$G(t_N) = \frac{2\lambda}{\sqrt{\pi\kappa\Delta t}} \sum_{i=1}^{N-1} \left[ (T_{i+1} - T_i) \left( \sqrt{N-i} - \sqrt{N-i+1} \right) \right], \quad (8)$$

where,  $G$  is ground heat flux,  $\kappa$  is thermal diffusivity,  $\lambda$  is thermal conductivity,  $\Delta T$  is the size of the time step, and  $T_i$  is the value of the temperature history at time step  $i$ . This equation is applied to ground surface temperature histories retrieved from SVD, PPI, and BTI techniques to estimate ground heat flux histories, with a range of plausible values for thermal conductivity and thermal diffusivity in the BTI case (Table 1).

### 3.7 Global averages

Global estimates of ground surface temperature from individual Xibalbá STPs are retrieved using the SVD, PPI, and BTI techniques. Global estimates from individual SVD inversions are obtained by averaging temperature and flux histories from each individual log, while the global uncertainty corresponds to the mean of the inversions of the extremal anomaly profiles. That is, the two extremal anomaly profiles derived by subtracting and adding the two sigma values of  $T_0$  and  $\Gamma_0$  to the best estimate of these parameters are inverted for each profile, constituting the upper and lower limits of the uncertainty range for the ground surface temperature history retrieved using the best estimate of  $T_0$  and  $\Gamma_0$  (i.e., the red and blue lines in Fig. 1). The mean of all the upper limits (red line) and the mean of all the lower limits (blue line) estimated from the 1079 Xibalbá profiles constitute the uncertainty range for the global average. A similar approach is applied in the case of individual PPI solutions, but the 2.5th, 50th, and 97.5th percentiles of each STP in the Xibalbá dataset are averaged. That is, the means of all

**Table 1.** Summary of the values for inversion parameters used to invert the artificial profile and logs from Xibalbá dataset. Columns contain the technique employed, the length of the time step used to retrieve the surface histories, the number of eigenvalues retrieved in the inversions, the values of thermal diffusivity considered, the values of thermal conductivity used to derive ground heat flux histories, the size of the Sampling ensemble of the BTI approach (in this case, the number of profiles considered,  $N_S$ ), and the size of the Bootstrapping ensemble of the BTI approach ( $N_B$ ). All combination of parameters are explored in each case.

Technique	Step change	Eigenvalues	Diffusivity	Conductivity	$N_S$	$N_B$
Artificial profile						
SVD	10, 30, 50 years	2, 3	$1 \times 10^{-6} \text{ m}^2 \text{ s}^{-1}$	–	–	–
PPI	10, 30, 50 years	2, 3	From $0.5 \times 10^{-6} \text{ m}^2 \text{ s}^{-1}$ to $1.5 \times 10^{-6} \text{ m}^2 \text{ s}^{-1}$ ( $N = 100$ )	–	–	–
BTI	10, 30, 50 years	2, 3	From $0.5 \times 10^{-6} \text{ m}^2 \text{ s}^{-1}$ to $1.5 \times 10^{-6} \text{ m}^2 \text{ s}^{-1}$ ( $N = 1000$ )	–	1	10, 100, 1000, 10 000, 100 000, 1 000 000
Xibalbá dataset						
SVD	10, 30, 50 years	2, 3	$1 \times 10^{-6} \text{ m}^2 \text{ s}^{-1}$	$3 \text{ W m}^{-1} \text{ K}^{-1}$	–	–
PPI	10, 30, 50 years	2, 3	From $0.5 \times 10^{-6} \text{ m}^2 \text{ s}^{-1}$ to $1.5 \times 10^{-6} \text{ m}^2 \text{ s}^{-1}$ ( $N = 100$ )	$3 \text{ W m}^{-1} \text{ K}^{-1}$	–	–
BTI	10, 30, 50 years	2, 3	From $0.5 \times 10^{-6} \text{ m}^2 \text{ s}^{-1}$ to $1.5 \times 10^{-6} \text{ m}^2 \text{ s}^{-1}$ ( $N = 1000$ )	From $2.5 \text{ W m}^{-1} \text{ K}^{-1}$ to $3.3 \text{ W m}^{-1} \text{ K}^{-1}$ ( $N = 1000$ )	1079	10, 100, 1000, 10 000

50th percentiles are considered to be the global averaged history, and the interval given by the means of all 2.5th and all 97.5th percentiles are considered to be the corresponding uncertainty range. These approaches have been used in previous studies to derive global estimates of temperature and heat flux changes in the land surface from SVD and PPI inversions (Beltrami et al., 2015a, b; Cuesta-Valero et al., 2021c), although those are not correct statistical methods. As previously discussed, the BTI framework can yield results from any number of logs by modifying the size of the Sampling ensemble. Therefore, global averages of temperature histories are estimated by including an inversion from each of the 1079 Xibalbá STPs in the Sampling ensemble. The mean of these 1079 inversions constitutes one member of the Bootstrapping ensemble, which therefore consists of 1000 global averages, each one estimated from 1079 different inversions, one from each profile in the dataset. The final global results are obtained by computing the 2.5th, 50th, and 97.5th percentiles of the Bootstrapping ensemble. Furthermore, we have tested the effect of considering the effective number of spatial degrees of freedom in observed surface temperatures on the calculation of the global mean ground surface temperature histories, finding it to be negligible (see Supplement).

The same approaches are applied to ground heat flux histories from Xibalbá profiles to derive global averaged heat flux histories.

### 3.8 Inversion parameters

We apply the SVD, PPI, and BTI techniques described above to an artificial subsurface anomaly profile generated from the PAGES2k-Land temperatures (Fig. 1a) and to the 1079 worldwide subsurface temperature profiles included in the Xibalbá database. We consider a range of possible values for each relevant parameter (see Table 1) in order to determine the uncertainty rising from poorly known quantities in the inversions.

The continental subsurface is considered to be homogeneous for all inversions performed here; thus, we assume no variation of the diffusivity or conductivity with depth. For SVD inversions, we use a constant thermal diffusivity of  $1 \times 10^{-6} \text{ m}^2 \text{ s}^{-1}$ , which is a typical value for these types of inversions (e.g., Hartmann and Rath, 2005; Jaume-Santero et al., 2016; Pickler et al., 2016, 2018). Thermal conductivity is also considered to be constant through the subsurface, with a value of  $3 \text{ W m}^{-1} \text{ K}^{-1}$  that also matches the conductivity

used in other works based on SVD inversions (Cermak and Rybach, 1982; Beltrami, 2001; Beltrami et al., 2002; Beltrami, 2002; Cuesta-Valero et al., 2021c). For the PPI and BTI approaches, we consider a range of thermal diffusivities from  $0.5 \times 10^{-6}$  to  $1.5 \times 10^{-6} \text{ m}^2 \text{ s}^{-1}$ . The BTI technique also takes into account a range of thermal conductivities from 2.5 to  $3.5 \text{ W m}^{-1} \text{ K}^{-1}$  to estimate ground heat fluxes from temperature histories (Eq. 8). Nevertheless, the PPI approach considers a constant thermal conductivity of  $3 \text{ W m}^{-1} \text{ K}^{-1}$  for estimating flux histories in order to simplify the comparison with results from SVD inversions. The considered ranges for thermal diffusivity and thermal conductivity for BTI inversions contain all plausible values addressed by the literature (Shen et al., 1995; Harris and Chapman, 2005; Hartmann and Rath, 2005; Woodbury and Ferguson, 2006; Chouinard et al., 2007; Hopcroft et al., 2007; Huang et al., 2008; Hopcroft et al., 2009; Davis et al., 2010; Rath et al., 2012; Demezhko and Gornostaeva, 2015b; Burton-Johnson et al., 2020).

All SVD, PPI, and BTI inversions use the same model for the boundary condition, i.e., the temporal signal at the surface, consisting of a series of step changes, all with the same temporal length. We perform inversions with time steps of 10, 30, and 50 years to test the effect of this parameter on the results produced by the three techniques. We also obtain SVD, PPI, and BTI inversions retaining the two and three largest eigenvalues in the decomposition matrix (Eq. 7) in order to test the dependency of the retrieved histories on this parameter.

## 4 Results

### 4.1 Methodological evaluation

An artificial profile generated from a known surface temperature allows one to evaluate the ability of the SVD, PPI, and BTI techniques described above to retrieve the original surface signal under perfect conditions (Fig. 1). Ground surface temperature histories obtained by applying the SVD and PPI methodologies recover the main features of the PAGES2k-Land temperatures used as surface boundary condition to generate the artificial profile (purple and red lines in Fig. 3). Inversions using two and three eigenvalues present similar temperature histories as well as similar uncertainty ranges, except at the end of the period when inversions performed with 10-year step changes in the surface signal with two eigenvalues yield larger uncertainties than inversions with three eigenvalues. Bootstrap inversions show similar temperature histories to those from SVD and PPI inversions, with uncertainty ranges slightly larger than those from SVD inversions and slightly lower than those from PPI inversions (Fig. 3). This is an expected result, as the BTI approach considers a range of possible values for thermal diffusivity, while SVD inversions consider only one value for diffusivity (Ta-

ble 1). Also, PPI uncertainty ranges are expected to be larger than BTI confidence intervals, because the PPI approach considers the two sigma values in long-term surface temperature and geothermal gradient for determining the two extremal anomaly profiles (red and blue dots in Fig. 1b). That is, the extremal anomalies in the PPI method are always going to represent a highly improbable case of the Gaussian distribution of possible values for long-term surface temperature and geothermal gradient, while the BTI approach samples randomly the possible anomalies given by a Gaussian distribution around the regression line obtained to estimate the quasi-equilibrium profile; thus, the 2.5th and 97.5th percentiles for the BTI inversions are always contained in the inversions of the extremal anomalies in the PPI case.

Small differences in ground surface temperature histories are present in 30-year (Fig. 3c) and 50-year (Fig. 3e) time step inversions retaining the two largest eigenvalues in the solution (Eq. 7). More importantly, the averaged ground surface temperature histories from inversions with time steps of 50-years and three eigenvalues show negative temperature changes around 1925 CE in SVD, PPI, and BTI cases, while the original surface temperature increases during the same period (Fig. 3f). This suggests that the third eigenvalue may be excessively small, leading to an unrealistic level of variability in the solutions of Eq. (7).

Results from the new bootstrap technique generally recover the original surface temperature used to derive the artificial profile (Fig. 3). The ground surface temperature histories retrieved by the BTI method, nevertheless, present a new parameter that affects the behavior of the retrieved histories: the size of the Bootstrapping ensemble (see Fig. 2, Table 1). The bootstrap approach is based on randomly sampling with repetition a number of different populations from the original, finite data (Efron, 1987; DiCiccio and Efron, 1996; Davison and Hinkley, 1997). An estimate of the probability density function for the desired statistic is then retrieved from these different populations, but the number of populations (i.e., the size of the Bootstrapping ensemble) is going to determine the final results. In the case of the retrieved temperature history from the artificial profile, we used a Bootstrapping ensemble with 1000 members, and an increase in the number of populations considered does not change the results (Fig. 4a). The retrieved uncertainty range is also sensible to the size of the Bootstrapping ensemble, but considering more than 1000 populations does not change the estimated uncertainty much (Fig. 4c).

### 4.2 Inverting the Xibalbá database

Inversions of the artificial profile have shown that the SVD, PPI, and BTI methods are able to yield very similar averaged ground surface temperature histories for one log, in agreement with the prescribed surface temperatures. However, this is a theoretical case, and real case applications would involve more complex situations, including a higher number

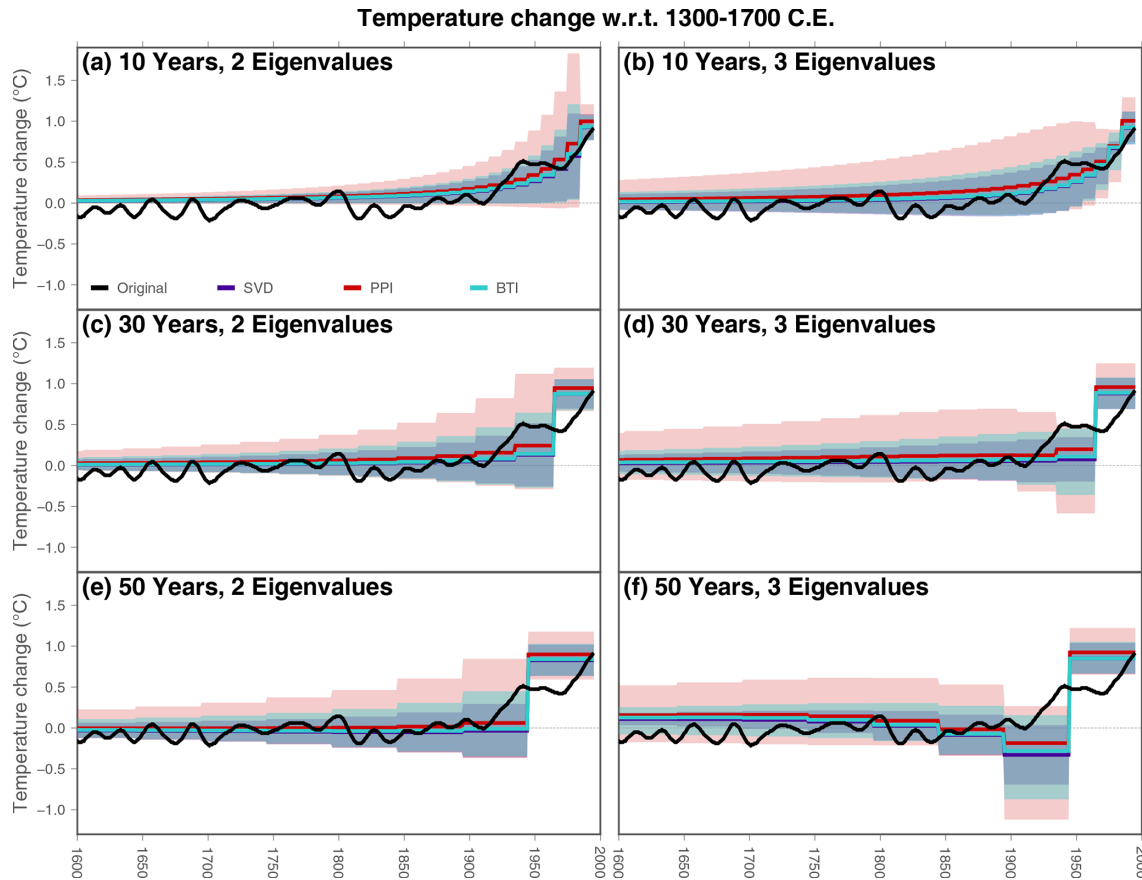


**Figure 3.** Ground surface temperature histories from the artificial profile using different step lengths for retrieving the surface signal (rows) and retaining different number of eigenvalues (columns). Colors indicate the method employed for the estimates: SVD (purple), PPI (red), and BTI (light blue). BTI results are derived using a Sampling ensemble of one member (the artificial profile) and a Bootstrapping ensemble of 1000 members. Shadows indicate the uncertainty range for each method. The original surface signal is represented in black.

of profiles with more noisy temperature records. This section describes the results obtained from the application of these three techniques to the subsurface temperature profiles from the Xibalbá dataset, including the comparison with global land temperatures estimated from PAGES2k multiproxy reconstructions and previous estimates from Cuesta-Valero et al. (2021c). Global ground heat flux histories are also retrieved and compared with estimates from Cuesta-Valero et al. (2021c).

Global averaged ground surface temperature histories from the Xibalbá dataset retrieved from the SVD, PPI, and BTI techniques are very similar for inversions considering time steps of 10, 30, and 50 years for the surface history and for inversions retaining the largest two and three eigenvalues (Fig. 5). The most important difference between inversion methods is the estimated uncertainty ranges, with PPI results yielding the broadest interval and BTI inversions the narrowest interval. In fact, the uncertainty range of the bootstrap approach is much smaller than that from SVD and PPI inversions for the global case, which is in contrast with the similar values achieved by the three techniques for the ar-

tificial profile (Fig. 3). This is caused by the differences in the methods used to estimate global uncertainties in the three approaches (see Sect. 3.7). The SVD and PPI methods aggregate the uncertainty of individual profiles to derive global uncertainty estimates. Concretely, these approaches average the upper and lower bounds of the individual uncertainty ranges, which provide a conservative global uncertainty range. That is, it is highly probable that the global averaged ground surface temperature history is contained in this interval, because it is markedly broad by construction. Nevertheless, this uncertainty range is not interpretable statistically, thus hindering its assessment against other past temperature estimates from STP inversions using Bayes methods, climate simulations, or proxy-based reconstructions. In contrast, the bootstrapping approach provides a meaningful statistical framework to derive global uncertainties. That is, the global uncertainty range retrieved by the BTI technique can be interpreted as the 95 % confidence interval of the global averaged ground surface temperature history, as it considers different possible values of the global average estimated using different, but possible, values for the unknown parameters in the inversion.

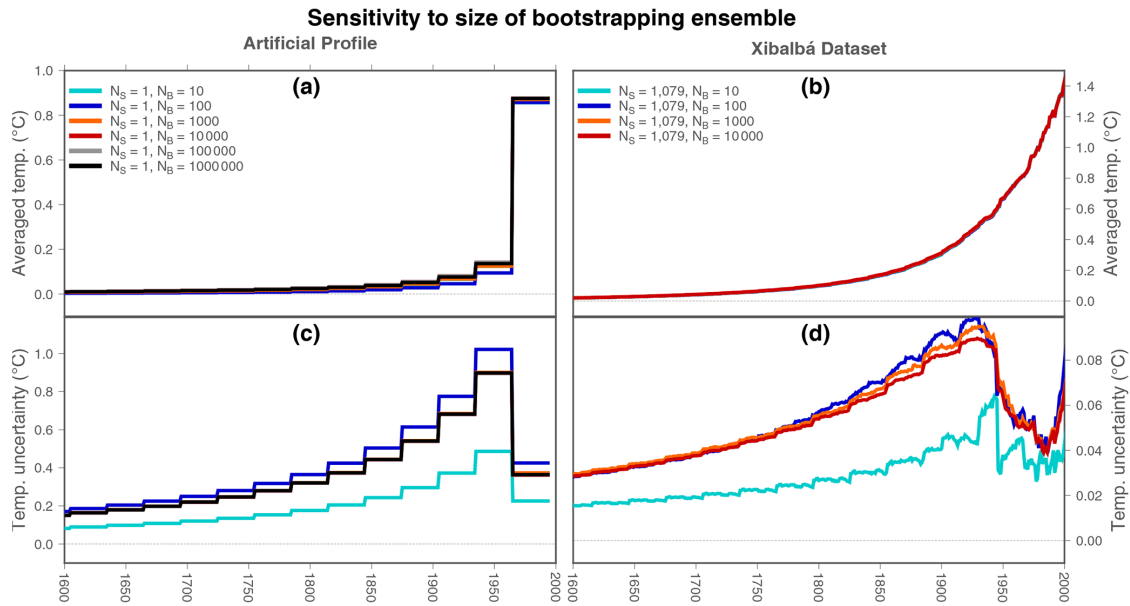


**Figure 4.** Temperature histories and uncertainty ranges in bootstrap inversions for different number of realizations. **(a)** Temperature histories for inversions of the artificial profile considering a population of one log (the artificial profile) ( $N_S = 1$ ) and a different number of realizations ( $N_B$  from 10 to 1 000 000). **(b)** Temperature histories for inversions of the Xibalbá dataset considering a population of 1079 logs ( $N_S = 1079$ ) and a different number of realizations ( $N_B$  from 10 to 10 000). **(c)** Uncertainty range for inversions of the artificial profile considering the same sizes for the Sampling and Bootstrapping ensembles as in **(a)**. **(d)** Uncertainty range for inversions of the Xibalbá dataset considering the same sizes for the Sampling and Bootstrapping ensembles as in **(b)**.

Therefore, results from the SVD and PPI techniques overestimate the global uncertainty due to an inadequate aggregation of individual uncertainties.

As in the case of the artificial profile, BTI results are sensitive to the number of re-samplings considered, i.e., the size of the Bootstrapping ensemble (Fig. 2). The dependency on the size of the Bootstrapping ensemble of the global averaged temperature history and the global uncertainty range from Xibalbá profiles converges to a stable value when the number of samplings increases, with small changes after considering a Bootstrapping ensemble of 1000 members (Fig. 4b and d). Considering more than 1000 ensemble members, therefore, does not change the results much; thus, 1000 is the recommended size for the Bootstrapping ensemble when applying the BTI technique to individual profiles and large sets of profiles, given the results of Fig. 4.

Global averaged ground heat flux histories estimated from Xibalbá profiles show similar results using the SVD, PPI, and BTI methods (Fig. 6). There is an unexpected decrease in the heat flux at the end of the 20th century for solutions considering 10-year step changes at the surface (Fig. 6a, b), which is not present in solutions with 30-year and 50-year time steps nor in previous estimates of global heat flux histories (Beltrami et al., 2002; Beltrami, 2002; Cuesta-Valero et al., 2021c). Furthermore, this flux decrease is present in all three methods retaining the two and three largest eigenvalues in the inversions, indicating that a 10-year step change

in the model for surface boundary conditions may be excessively small, at least to retrieve past histories of ground heat flux. There are also differences in the retrieved uncertainty range for the global mean from each technique, with BTI results displaying a much smaller uncertainty than SVD and PPI results. This is an expected result, since the ground heat flux histories from the three inversion methods are estimated from ground surface temperature histories, which also yielded these differences in the retrieved uncertainty range (Fig. 5).

The assessment of ground surface temperature histories retrieved from Xibalbá STPs using the SVD, PPI, and BTI methods shows agreement with previous estimates from the same logs retrieved with a slightly different PPI technique (Fig. 7a and Table 2). The main methodological difference between the PPI approach used here and the approach used in Cuesta-Valero et al. (2021c) consists of filtering individual inversions to remove unrealistic histories in comparison with long-term changes in meteorological data. This additional screening removed the histories showing the largest variability with time, reducing the uncertainty range in the estimates of ground heat flux histories and ground surface temperature histories. Therefore, the lack of filtering in the PPI approach applied here explains the smaller uncertainty range in Cuesta-Valero et al. (2021c). Another remarkable result is the agreement in the temporal evolution of the PAGES2k-Land temperatures and the ground surface temperature histories

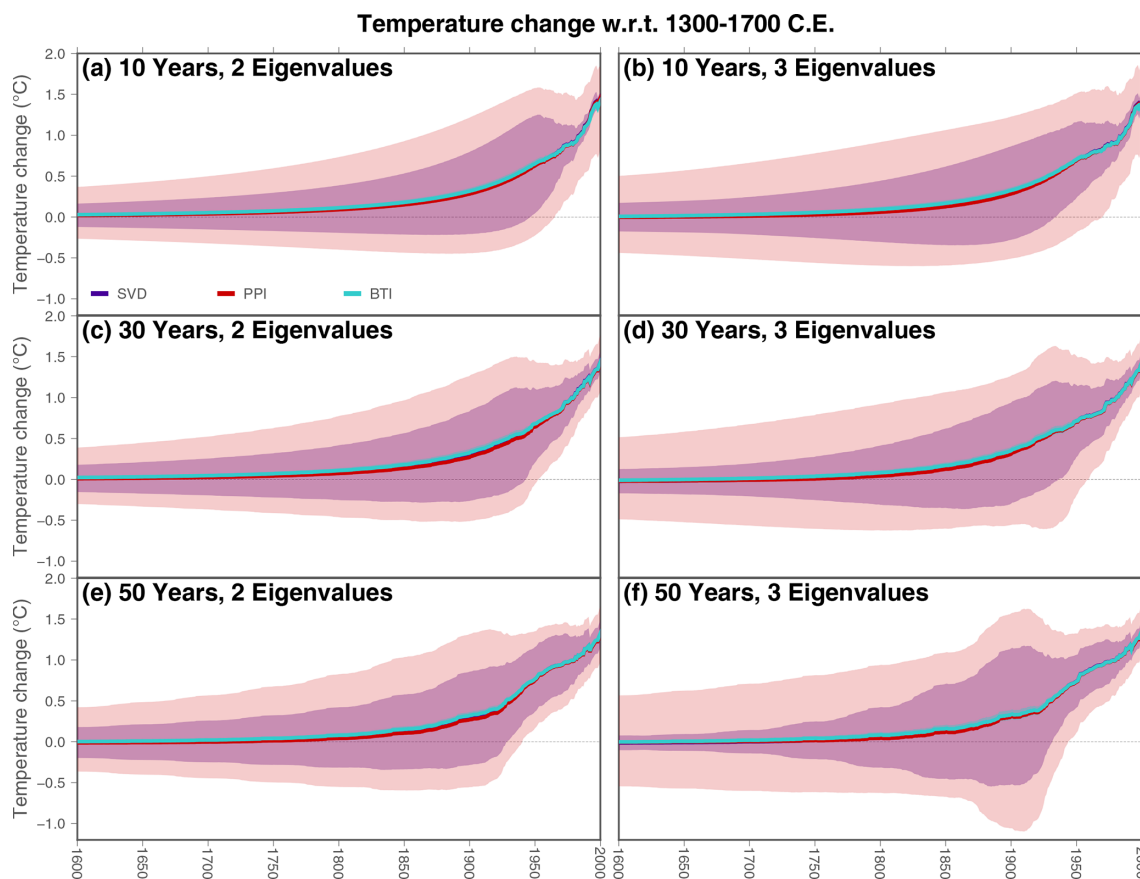


**Figure 5.** Global averaged ground surface temperature histories from Xibalbá profiles using different step lengths for retrieving the surface signal (rows) and retaining different numbers of eigenvalues (columns). Colors indicate the method employed for the estimates: SVD (purple), PPI (red), and BTI (light blue). BTI results are derived using a Sampling ensemble of 1079 members and a Bootstrapping ensemble of 1000 members. Shadows indicate the uncertainty range for each method. Note that the uncertainty in BTI results is represented, although difficult to visualize due to its small size.

(Fig. 7a). However, this agreement is not visible in the magnitude of temperature changes, particularly after 1800 CE., because of a temperature decrease recorded in the PAGES2k-Land dataset in 1820 CE. that is not captured in the STP inversions, which leads to smaller mean temperature changes from PAGES2k-land data than from the Xibalbá profiles from around 1800 to 2000 CE (Table 2). Nevertheless, similar temperature trends can be observed for both proxy and STP datasets during this period. This difference in warming from multi-proxy data and subsurface temperature profiles is a known problem that needs further investigation in order to reconcile the estimated temperature evolution during the last millennium from both datasets. Nevertheless, results in Fig. 7a show smaller differences than expected in comparison with previous analyses (Huang et al., 2000; Harris and Chapman, 2005; Jaume-Santero et al., 2016; Beltrami et al., 2017). PAGES2k-Land temperatures have been horizontally displaced to have the same period of reference as the STP inversions – that is, 1300–1700 CE. Therefore, the small offset around 1600 CE is just caused by the natural variability of

the PAGES2k series, which includes higher-frequency signals than STP results.

The averaged ground heat flux histories derived here are also in agreement with those from Cuesta-Valero et al. (2021c) despite several methodological differences (Fig. 7b). As indicated above, the PPI method in Cuesta-Valero et al. (2021c) removed individual inversions with high variability from the PPI ensemble, sampled a range of possible conductivities, and weighted each inversion in comparison with the measured profile. These three factors, particularly the sampling of a range of conductivities, lead to higher uncertainty in Cuesta-Valero et al. (2021c) than in the PPI ground heat flux histories retrieved here.

## 5 Discussion

The new BTI technique, based on combining a broadly used SVD algorithm with a bootstrap sampling approach, presents robust estimates of ground temperature histories and ground heat flux histories in comparison with results from the SVD

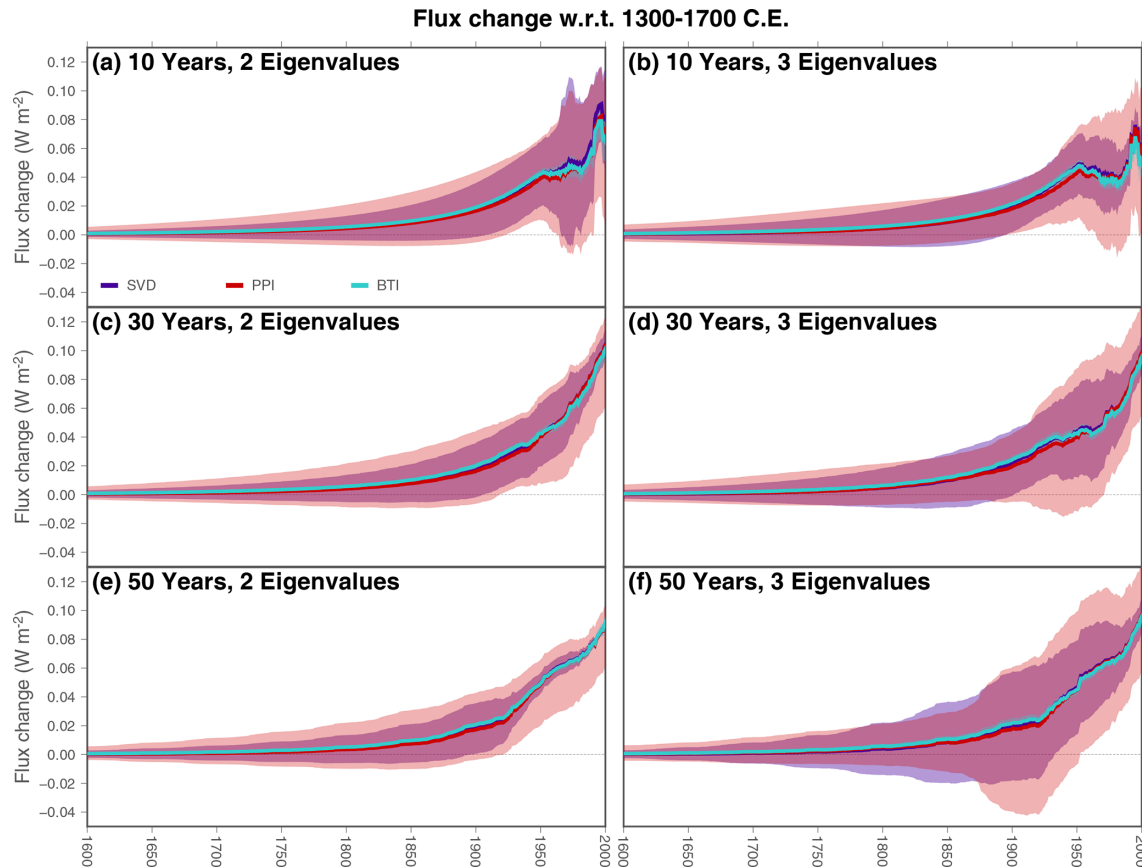


**Figure 6.** Global averaged ground heat flux histories from Xibalbá profiles using different step lengths for retrieving the surface signal (rows) and retaining different numbers of eigenvalues (columns). Colors indicate the method employed for the estimates: SVD (purple), PPI (red), and BTI (light blue). BTI results are derived using a Sampling ensemble of 1079 members and a Bootstrapping ensemble of 1000 members. Shadows indicate the uncertainty range for each method. Note that the uncertainty in BTI results is represented, although it is difficult to visualize due to its small size.

**Table 2.** Averaged ground surface temperature histories and averaged ground heat flux histories retrieved using the SVD, PPI, and BTI techniques described in the Methods section. Temperature changes from the PAGES2k-Land temperatures and temperature and flux histories from Cuesta-Valero et al. (2021c) (CV21) are also shown for comparison purposes. Results from the BTI technique consider  $N_S = 1079$  and  $N_B = 1000$ . Temperatures in  $^{\circ}\text{C}$ , fluxes in  $\text{W m}^{-2}$ .

Period CE	Temperature					Heat flux			
	PAGES2k	CV21	SVD	PPI	BTI	CV21	SVD	PPI	BTI
1950–2000	$0.57 \pm 0.18$	$1.00 \pm 0.25$	$1.01 \pm 0.30$	$1.0 \pm 0.5$	$1.008 \pm 0.025$	$0.065 \pm 0.033$	$0.068 \pm 0.005$	$0.067 \pm 0.022$	$0.0672 \pm 0.0028$
1900–1950	$0.22 \pm 0.19$	$0.5 \pm 0.5$	$0.5 \pm 0.5$	$0.5 \pm 0.8$	$0.50 \pm 0.04$	$0.03 \pm 0.04$	$0.030 \pm 0.013$	$0.029 \pm 0.023$	$0.0318 \pm 0.0018$
1850–1900	$-0.00 \pm 0.20$	$0.2 \pm 0.4$	$0.2 \pm 0.5$	$0.2 \pm 0.9$	$0.22 \pm 0.04$	$0.012 \pm 0.030$	$0.012 \pm 0.015$	$0.011 \pm 0.022$	$0.0143 \pm 0.0014$
1800–1850	$-0.07 \pm 0.21$	$0.09 \pm 0.29$	$0.1 \pm 0.4$	$0.1 \pm 0.7$	$0.110 \pm 0.032$	$0.008 \pm 0.020$	$0.005 \pm 0.011$	$0.005 \pm 0.018$	$0.0071 \pm 0.0011$
1750–1800	$0.03 \pm 0.24$	$0.03 \pm 0.26$	$0.03 \pm 0.33$	$0.0 \pm 0.6$	$0.057 \pm 0.026$	$0.005 \pm 0.022$	$0.003 \pm 0.008$	$0.002 \pm 0.014$	$0.0039 \pm 0.0008$
1700–1750	$-0.06 \pm 0.27$	$-0.01 \pm 0.25$	$0.01 \pm 0.28$	$0.0 \pm 0.5$	$0.030 \pm 0.022$	$0.004 \pm 0.024$	$0.001 \pm 0.006$	$0.001 \pm 0.011$	$0.0023 \pm 0.0006$
1650–1700	$-0.06 \pm 0.34$	$-0.03 \pm 0.25$	$-0.00 \pm 0.23$	$-0.0 \pm 0.5$	$0.014 \pm 0.019$	$0.003 \pm 0.025$	$0.001 \pm 0.004$	$0.001 \pm 0.008$	$0.0013 \pm 0.0004$
1600–1650	$-0.1 \pm 0.4$	$-0.04 \pm 0.24$	$-0.01 \pm 0.20$	$-0.0 \pm 0.4$	$0.005 \pm 0.017$	$0.003 \pm 0.025$	$0.0004 \pm 0.0031$	$0.000 \pm 0.006$	$0.00078 \pm 0.00031$

and PPI methods, both for an artificial case and for real STPs. A number of possible values for several inversion parameters are considered, including different lengths of the time steps for retrieving the surface histories and the number of eigenvalues retained in the inversion, with all cases showing BTI results in agreement with the SVD and PPI techniques. The

effect of considering different lengths for the time steps to retrieve surface histories is small, consisting of lower temperature changes with increasing time steps, since solutions retrieve the averaged surface signal for a longer period of time. Nevertheless, there are some unrealistic results when considering 10-year time steps and when retaining the three

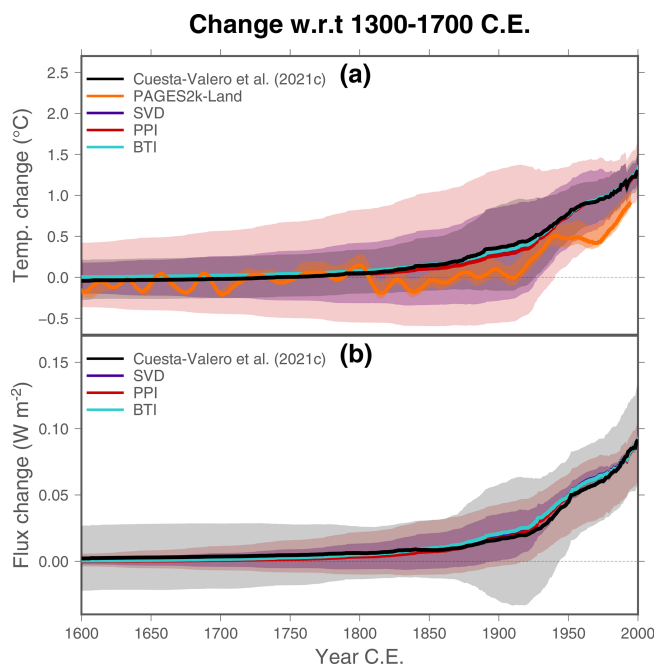


**Figure 7.** (a) Ground surface temperature histories from the three techniques analyzed here using the Xibalbá dataset in comparison with previous results from Cuesta-Valero et al. (2021c) (black) and the PAGES2k-Land temperatures (orange). (b) Ground heat flux histories from the three techniques analyzed here using the Xibalbá dataset in comparison with results from Cuesta-Valero et al. (2021c) (black). Results from the BTI technique in both panels consider Sampling and Bootstrapping ensembles with 1079 and 1000 members, respectively. Note that the uncertainty in BTI results is represented, although difficult to visualize due to its small size.

largest eigenvalues in the solution. Therefore, inversions performed with 30-year and 50-year time steps retaining the two largest eigenvalues in the solutions are more adequate for inverting STPs from the Xibalbá global dataset, but the time step and the number of retained eigenvalues should be selected on a case-by-case basis, depending on the application of interest.

The most important difference of the new bootstrap technique compared to previous methods arises when aggregating the retrieved inversions to estimate the global mean temperature history and the global mean heat flux history, as the uncertainty range derived in this case is markedly smaller for BTI results to that for SVD and PPI results. The SVD and PPI techniques average the upper and lower limits of the uncertainty range of all profiles (red and blue lines in Fig. 1a) to provide an estimate of the global uncertainty, while the bootstrap technique derives a high number (1000 in this study) of different global means, from which the 2.5th and 97.5th percentiles are estimated. In other words, the global uncertainties from the SVD and PPI techniques are conceptually different from the uncertainty estimated from the BTI technique. In fact, the SVD and PPI uncertainties are difficult to

interpret using standard statistical paradigms, while the uncertainty estimates of the BTI approach follow the general principles of bootstrapping. However, the global uncertainty from the SVD and PPI methods converges to that of the bootstrap approach if considering the uncertainty from the inversion of individual logs as Gaussian errors and applying standard error propagation (Fig. 8). That is, if uncertainty in SVD and PPI inversions from individual profiles is considered to be Gaussian, the standard error of each individual log can be used to derive a standard error for the global mean using typical error propagation methods instead of averaging the limits of the uncertainty range. Figure 8 displays the uncertainty ranges for the global averaged temperature and heat flux histories estimated by standard error propagation of individual SVD and PPI results as well as the confidence interval from the bootstrapping approach. The uncertainty ranges from the three techniques present very similar values for the entire period of interest when considering a common value of thermal diffusivity and conductivity. However, the retrieved errors in individual SVD and PPI inversions do not follow, in general, a Gaussian distribution (see uncertainty ranges in Fig. 3); thus, the use of standard error propagation techniques with the SVD and PPI solutions is not advised. In contrast, the BTI method does not make any assumption regarding the distribution of random errors, which is an advantage for aggregating individual inversions. Another factor leading to the small confidence intervals for the global mean surface temperature and heat flux histories achieved by the BTI technique is the lack of high-frequency signals in inversions of subsurface temperature profiles. As explained in the Methods section, the ground acts as a filter, removing the short-period alterations in the surface energy balance; thus, measured STPs only retain long-term changes in surface conditions (e.g., Smerdon and Stieglitz, 2006). Thereby, STP inversions contain only long-term variability, reducing the uncertainty in the retrieved surface histories. Overall, we conclude that the bootstrap technique is a more adequate method for aggregating results from individual subsurface temperature profiles from a statistical point of view, and it provides more interpretable and meaningful uncertainty estimates for global averages than the typical SVD and PPI approaches.

The similar global histories of ground surface temperature and ground heat flux for the three methods assessed here indicate that the ground component of the Earth's heat inventory and the estimated temperature change since preindustrial times from STP inversions using the bootstrap method are also similar to previous results. Ground heat flux from the bootstrap technique yields  $67.2 \text{ W m}^{-2}$  for the period 1950–2000 CE (Table 2), which correspond to a global ground heat storage of  $14 \times 10^{21} \text{ J}$ , in agreement with the results of von Schuckmann et al. (2020). The global temperature change since preindustrial times – around 1300–1700 CE, in this case (Cuesta-Valero et al., 2019) – can be estimated by assuming that land surface temperature changes are around 2.36 times larger than sea surface temperature

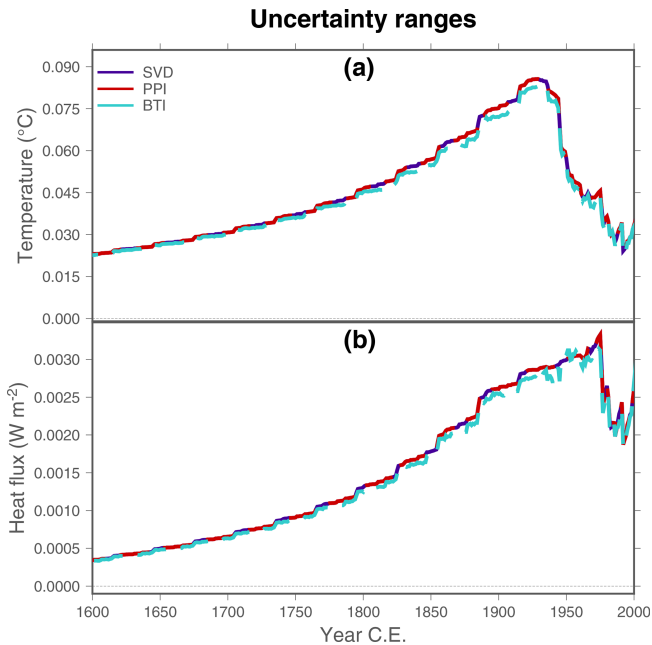


**Figure 8.** Uncertainty ranges for the three techniques analyzed here, using error propagation to estimate the uncertainties in the SVD and PPI global averages. **(a)** Uncertainty ranges of the global averaged temperature histories from Xibalbá subsurface temperature profiles using error propagation of SVD and PPI inversions (purple and red lines) and standard BTI inversions (light blue lines). **(b)** Uncertainty range of the global averaged heat flux histories from Xibalbá subsurface temperature profiles using error propagation of SVD and PPI inversions (purple and red lines) and standard BTI inversions (light blue lines). All results were obtained considering constant thermal diffusivity and conductivity; thus, differences are caused only due to the different aggregation techniques.

changes (Harrison et al., 2015), thus obtaining an increase of 0.7 °C in the global temperature. That is the same estimate as in Cuesta-Valero et al. (2021c) using Xibalbá profiles. However, the uncertainty in estimates performed using the BTI technique is smaller than in previous results by an order of magnitude (Table 2). This is relevant to assess the total uncertainty in the Earth’s heat inventory and to compare with other components of the continental heat storage, such as inland water bodies (Vanderkelen et al., 2020). Furthermore, the uncertainty range of the temperature changes since preindustrial times from subsurface temperature profiles is now smaller than the uncertainty in estimates from other sources (0.6–0.8 °C, Hawkins et al., 2017).

## 6 Conclusions

A new bootstrap technique to quantify uncertainties in SVD inversions of subsurface temperature profiles has been described and tested, obtaining robust results in comparison with other methods. This new technique reaches similar val-

ues of ground heat storage and temperature change since preindustrial times compared to previous studies, although it provides more meaningful uncertainty ranges. The bootstrap method is able to incorporate several important sources of uncertainty affecting the inversion of subsurface temperature profiles in a flexible framework that allows the analysis of individual profiles as well as the analysis of datasets with thousands of profiles, and it is based on robust statistical paradigms.

As expected, the new bootstrap approach estimates lower uncertainties for global histories of surface temperature and heat flux than other inversion methods. This result reinforces the role of inversions of subsurface temperature profiles as indicators of long-term changes in surface conditions and thus the importance of expanding the global network of profiles to include measurements in the southern hemisphere, the Middle East, and southeastern Asia as well as to include more recent measurements at previously sampled sites in order to include the recent land warming in global estimates from inversions of subsurface temperature profiles.

*Code and data availability.* The CIBOR collection of scripts is available at Zenodo (<https://doi.org/10.5281/zenodo.7152900>, Cuesta-Valero, 2022). Xibalbá temperature profiles are available from <https://doi.org/10.6084/m9.figshare.13516487.v4> (Cuesta-Valero et al., 2021a). Multi-proxy temperatures were retrieved from the data associated with the Summary for Policymakers of the sixth Assessment Report of the IPCC (IPCC, 2021).

*Supplement.* The supplement related to this article is available online at: <https://doi.org/10.5194/gmd-15-7913-2022-supplement>.

*Author contributions.* FJCV wrote the paper with continuous feedback from all authors. FJCV performed all calculations and produced all figures in this study. FJCV, HB, SG, AGG, and JFGR participated in the design of the study and in the development of the bootstrapping technique. All authors read the final version of the paper.

*Competing interests.* The contact author has declared that none of the authors has any competing interests.

*Disclaimer.* Publisher’s note: Copernicus Publications remains neutral with regard to jurisdictional claims in published maps and institutional affiliations.

*Acknowledgements.* We thank two anonymous reviewers for their constructive feedback. Francisco José Cuesta-Valero is an Alexander von Humboldt Research Fellow at the Helmholtz Centre for Environmental Research (UFZ). Hugo Beltrami holds the Canada Research Chair in Climate Dynamics, and Stephan Gruber holds

the Canada Research Chair in Climate Change Impacts/Adaptation in Northern Canada. This work was partially supported by grants from the Natural Sciences and Engineering Research Council of Canada. Part of the presented analysis was performed in the computational facilities provided by the Atlantic Computational Excellence Network (ACENET-Compute Canada). This analysis contributes to the PALEOLINK project (<https://pastglobalchanges.org/science/wg/2k-network/projects/paleolink/intro>, last access: 9 February 2022), part of the PAGES 2k Network.

*Financial support.* This research has been supported by the Alexander von Humboldt-Stiftung (Research Fellowship grant), the Canada Research Chairs Program, and the Natural Sciences and Engineering Research Council of Canada Discovery Grants (NSERC DG 140576948 and 2020-04783).

The article processing charges for this open-access publication were covered by the Helmholtz Centre for Environmental Research – UFZ.

*Review statement.* This paper was edited by Chanh Kieu and reviewed by two anonymous referees.

## References

- Alexeev, V. A., Nicolsky, D. J., Romanovsky, V. E., and Lawrence, D. M.: An evaluation of deep soil configurations in the CLM3 for improved representation of permafrost, *Geophys. Res. Lett.*, 34, 109502, <https://doi.org/10.1029/2007GL029536>, 2007.
- Beltrami, H.: Surface heat flux histories from inversion of geothermal data: Energy balance at the Earth's surface, *J. Geophys. Res.-Sol. Ea.*, 106, 21979–21993, <https://doi.org/10.1029/2000JB000065>, 2001.
- Beltrami, H.: Climate from borehole data: Energy fluxes and temperatures since 1500, *Geophys. Res. Lett.*, 29, 2111, <https://doi.org/10.1029/2002GL015702>, 2002.
- Beltrami, H. and Mareschal, J.-C.: Ground temperature histories for central and eastern Canada from geothermal measurements: Little Ice Age signature, *Geophys. Res. Lett.*, 19, 689–692, <https://doi.org/10.1029/92GL00671>, 1992.
- Beltrami, H. and Taylor, A. E.: Records of climatic change in the Canadian Arctic: towards calibrating oxygen isotope data with geothermal data, *Global Planet. Change*, 11, 127–138, [https://doi.org/10.1016/0921-8181\(95\)00006-2](https://doi.org/10.1016/0921-8181(95)00006-2), 1995.
- Beltrami, H., Jessop, A. M., and Mareschal, J.-C.: Ground temperature histories in eastern and central Canada from geothermal measurements: evidence of climatic change, *Global Planet. Change*, 6, 167–183, [https://doi.org/10.1016/0921-8181\(92\)90033-7](https://doi.org/10.1016/0921-8181(92)90033-7), 1992.
- Beltrami, H., Smerdon, J. E., Pollack, H. N., and Huang, S.: Continental heat gain in the global climate system, *Geophys. Res. Lett.*, 29, 8-1–8-3, <https://doi.org/10.1029/2001GL014310>, 2002.
- Beltrami, H., Smerdon, J. E., Matharoo, G. S., and Nickerson, N.: Impact of maximum borehole depths on inverted temperature histories in borehole paleoclimatology, *Clim. Past*, 7, 745–756, <https://doi.org/10.5194/cp-7-745-2011>, 2011.
- Beltrami, H., Matharoo, G. S., and Smerdon, J. E.: Ground surface temperature and continental heat gain: uncertainties from underground, *Environ. Res. Lett.*, 10, 014009, <https://doi.org/10.1088/1748-9326/10/1/014009>, 2015a.
- Beltrami, H., Matharoo, G. S., and Smerdon, J. E.: Impact of borehole depths on reconstructed estimates of ground surface temperature histories and energy storage, *J. Geophys. Res.-Ea. Surf.*, 120, 763–778, <https://doi.org/10.1002/2014JF003382>, 2015b.
- Beltrami, H., Matharoo, G. S., Smerdon, J. E., Illanes, L., and Tarasov, L.: Impacts of the Last Glacial Cycle on ground surface temperature reconstructions over the last millennium, *Geophys. Res. Lett.*, 44, 355–364, <https://doi.org/10.1002/2016GL071317>, 2017.
- Burton-Johnson, A., Dziadek, R., and Martin, C.: Review article: Geothermal heat flow in Antarctica: current and future directions, *The Cryosphere*, 14, 3843–3873, <https://doi.org/10.5194/tc-14-3843-2020>, 2020.
- Carslaw, H. S. and Jaeger, J. C.: *Conduction of Heat in Solids*, Clarendon Press, Oxford, 1959.
- Cermak, V. and Rybach, L.: Thermal conductivity and specific heat of minerals and rocks, in: *Landolt Börnstein: Physical Properties of Rocks, Group V, Geophysics, Volume 1a*, edited by: Angenheister, G., Springer-Verlag Berlin Heidelberg, [https://doi.org/10.1007/10201894\\_62](https://doi.org/10.1007/10201894_62), 1982.
- Chouinard, C., Fortier, R., and Mareschal, J.-C.: Recent climate variations in the subarctic inferred from three borehole temperature profiles in northern Quebec, Canada, *Earth Planet. Sc. Lett.*, 263, 355–369, <https://doi.org/10.1016/j.epsl.2007.09.017>, 2007.
- Clauser, C. and Mareschal, J.-C.: Ground temperature history in central Europe from borehole temperature data, *Geophys. J. Int.*, 121, 805–817, <https://doi.org/10.1111/j.1365-246X.1995.tb06440.x>, 1995.
- Cuesta-Valero, F. J.: CIBOR: Codes for Inverting BOREholes (1.0.0), Zenodo [code], <https://doi.org/10.5281/zenodo.7152900>, 2022.
- Cuesta-Valero, F. J., García-García, A., Beltrami, H., and Smerdon, J. E.: First assessment of continental energy storage in CMIP5 simulations, *Geophys. Res. Lett.*, 43, 2016GL068496, <https://doi.org/10.1002/2016GL068496>, 2016.
- Cuesta-Valero, F. J., García-García, A., Beltrami, H., Zorita, E., and Jaume-Santero, F.: Long-term Surface Temperature (LoST) database as a complement for GCM preindustrial simulations, *Clim. Past*, 15, 1099–1111, <https://doi.org/10.5194/cp-15-1099-2019>, 2019.
- Cuesta-Valero, F. J., Beltrami, H., García-García, A., González-Rourco, J. F., and García-Bustamante, E.: Xibalbá: Underground Temperature Database, figshare [data set], <https://doi.org/10.6084/m9.figshare.13516487.v4>, 2021a.
- Cuesta-Valero, F. J., García-García, A., Beltrami, H., and Finnis, J.: First assessment of the earth heat inventory within CMIP5 historical simulations, *Earth Syst. Dynam.*, 12, 581–600, <https://doi.org/10.5194/esd-12-581-2021>, 2021b.
- Cuesta-Valero, F. J., García-García, A., Beltrami, H., González-Rourco, J. F., and García-Bustamante, E.: Long-term global ground heat flux and continental heat storage from geothermal data, *Clim. Past*, 17, 451–468, <https://doi.org/10.5194/cp-17-451-2021>, 2021c.

- Davis, M. G., Harris, R. N., and Chapman, D. S.: Repeat temperature measurements in boreholes from northwestern Utah link ground and air temperature changes at the decadal time scale, *J. Geophys. Res.-Sol. Ea.*, 115, B05203, <https://doi.org/10.1029/2009JB006875>, 2010.
- Davison, A. C. and Hinkley, D. V.: *Bootstrap Methods and their Application*, Cambridge University Press, Cambridge, United Kingdom, 1997.
- Demezhko, D. Y. and Gornostaeva, A. A.: Late Pleistocene–Holocene ground surface heat flux changes reconstructed from borehole temperature data (the Urals, Russia), *Clim. Past*, 11, 647–652, <https://doi.org/10.5194/cp-11-647-2015>, 2015a.
- Demezhko, D. Y. and Gornostaeva, A. A.: Reconstructions of ground surface heat flux variations in the urals from geothermal and meteorological data, *Izvestiya, Atmos. Ocean. Phys.*, 51, 723–736, <https://doi.org/10.1134/S0001433815070026>, 2015b.
- DiCiccio, T. J. and Efron, B.: Bootstrap confidence intervals, *Stat. Sci.*, 11, 189–228, <https://doi.org/10.1214/ss/1032280214>, 1996.
- Donohoe, A., Armour, K. C., Pendergrass, A. G., and Battisti, D. S.: Shortwave and longwave radiative contributions to global warming under increasing CO<sub>2</sub>, *P. Natl. Acad. Sci.*, 111, 16700–16705, <https://doi.org/10.1073/pnas.1412190111>, 2014.
- Efron, B.: Better Bootstrap Confidence Intervals, *J. Am. Stat. Assoc.*, 82, 171–185, <https://doi.org/10.1080/01621459.1987.10478410>, 1987.
- García-García, A., Cuesta-Valero, F. J., Beltrami, H., and Smerdon, J. E.: Simulation of air and ground temperatures in PMIP3/CMIP5 last millennium simulations: implications for climate reconstructions from borehole temperature profiles, *Environ. Res. Lett.*, 11, 044022, <https://doi.org/10.1088/1748-9326/11/4/044022>, 2016.
- González-Rouco, J. F., Beltrami, H., Zorita, E., and von Storch, H.: Simulation and inversion of borehole temperature profiles in surrogate climates: Spatial distribution and surface coupling, *Geophys. Res. Lett.*, 33, 101703, <https://doi.org/10.1029/2005GL024693>, 2006.
- González-Rouco, J. F., Beltrami, H., Zorita, E., and Stevens, M. B.: Borehole climatology: a discussion based on contributions from climate modeling, *Clim. Past*, 5, 97–127, <https://doi.org/10.5194/cp-5-97-2009>, 2009.
- González-Rouco, J. F., J.Steinert, N., E.García-Bustamante, Hagemann, S., de Vreseand J. H. Jungclaus, P., Lorenz, S. J., Melo-Aguilar, C., García-Pereira, F., and Navarro, J.: Increasing the Depth of a Land Surface Model. Part I: Impacts on the Sub-surface Thermal Regime and Energy Storage, *J. Hydrometeorol.*, 22, 3211–3230, <https://doi.org/10.1175/JHM-D-21-0024.1>, 2021.
- Hansen, J., Sato, M., Kharecha, P., and von Schuckmann, K.: Earth's energy imbalance and implications, *Atmos. Chem. Phys.*, 11, 13421–13449, <https://doi.org/10.5194/acp-11-13421-2011>, 2011.
- Harris, R. N. and Chapman, D. S.: Borehole temperatures and tree rings: Seasonality and estimates of extratropical Northern Hemispheric warming, *J. Geophys. Res.-Ea. Surf.*, 110, F04003, <https://doi.org/10.1029/2005JF000303>, 2005.
- Harrison, S. P., Bartlein, P. J., Izumi, K., Li, G., Annan, J., Hargreaves, J., Braconnot, P., and Kageyama, M.: Evaluation of CMIP5 palaeo-simulations to improve climate projections, *Nature Clim. Change*, 5, 735–743, <https://doi.org/10.1038/nclimate2649>, 2015.
- Hartmann, A. and Rath, V.: Uncertainties and shortcomings of ground surface temperature histories derived from inversion of temperature logs, *J. Geophys. Eng.*, 2, 299–311, <https://doi.org/10.1088/1742-2132/2/4/S02>, 2005.
- Hawkins, E., Ortega, P., Suckling, E., Schurer, A., Hegerl, G., Jones, P., Joshi, M., Osborn, T. J., Masson-Delmotte, V., Mignot, J., Thorne, P., and van Oldenborgh, G. J.: Estimating Changes in Global Temperature since the Preindustrial Period, *Bull. Am. Meteorol. Soc.*, 98, 1841–1856, <https://doi.org/10.1175/BAMS-D-16-0007.1>, 2017.
- Hermoso de Mendoza, I., Beltrami, H., MacDougall, A. H., and Mareschal, J.-C.: Lower boundary conditions in land surface models – effects on the permafrost and the carbon pools: a case study with CLM4.5, *Geosci. Model Dev.*, 13, 1663–1683, <https://doi.org/10.5194/gmd-13-1663-2020>, 2020.
- Hicks Pries, C. E., Castanha, C., Porras, R. C., and Torn, M. S.: The whole-soil carbon flux in response to warming, *Science*, 355, 1420–1423, <https://doi.org/10.1126/science.aal1319>, 2017.
- Hopcroft, P. O., Gallagher, K., and Pain, C. C.: Inference of past climate from borehole temperature data using Bayesian Reversible Jump Markov chain Monte Carlo, *Geophys. J. Int.*, 171, 1430–1439, <https://doi.org/10.1111/j.1365-246X.2007.03596.x>, 2007.
- Hopcroft, P. O., Gallagher, K., and Pain, C. C.: A Bayesian partition modelling approach to resolve spatial variability in climate records from borehole temperature inversion, *Geophys. J. Int.*, 178, 651–666, <https://doi.org/10.1111/j.1365-246X.2009.04192.x>, 2009.
- Huang, S., Pollack, H. N., and Shen, P.-Y.: Temperature trends over the past five centuries reconstructed from borehole temperatures, *Nature*, 403, 756–758, <https://doi.org/10.1038/35001556>, 2000.
- Huang, S. P., Pollack, H. N., and Shen, P.-Y.: A late Quaternary climate reconstruction based on borehole heat flux data, borehole temperature data, and the instrumental record, *Geophys. Res. Lett.*, 35, L13703, <https://doi.org/10.1029/2008GL034187>, 2008.
- IPCC: Summary for Policymakers, pp. 3–32, Cambridge University Press, Cambridge, United Kingdom and New York, NY, USA, [https://www.ipcc.ch/report/ar6/wg1/downloads/report/IPCC\\_AR6\\_WGI\\_SPM.pdf](https://www.ipcc.ch/report/ar6/wg1/downloads/report/IPCC_AR6_WGI_SPM.pdf) (last access: 28 October 2022), 2021.
- Jaume-Santero, F., Pickler, C., Beltrami, H., and Mareschal, J.-C.: North American regional climate reconstruction from ground surface temperature histories, *Clim. Past*, 12, 2181–2194, <https://doi.org/10.5194/cp-12-2181-2016>, 2016.
- Jaupard, C. and Mareschal, J. C.: *Heat generation and transport in the Earth*, Cambridge University Press, New York, 2010.
- Johnson, G. C., Lyman, J. M., and Loeb, N. G.: Improving estimates of Earth's energy imbalance, *Nat. Clim. Change*, 6, 639, <https://doi.org/10.1038/nclimate3043>, 2016.
- Kukkonen, I. T., Suhonen, E., Ezhova, E., Lappalainen, H., Gennadinik, V., Ponomareva, O., Gravis, A., Miles, V., Kulmala, M., Melnikov, V., and Drozdov, D.: Observations and modelling of ground temperature evolution in the discontinuous permafrost zone in Nady, north-west Siberia, *Permafrost and Periglacial Processes*, 31, 264–280, <https://doi.org/10.1002/ppp.2040>, 2020.
- Lanczos, C.: *Linear differential operators*, Van Nostrand, New York, 1961.
- MacDougall, A. H., Beltrami, H., González-Rouco, J. F., Stevens, M. B., and Bourlon, E.: Comparison of observed and general cir-

- ulation model derived continental subsurface heat flux in the Northern Hemisphere, *J. Geophys. Res.-Atmos.*, 115, D12109, <https://doi.org/10.1029/2009JD013170>, 2010.
- Mareschal, J.-C. and Beltrami, H.: Evidence for recent warming from perturbed geothermal gradients: examples from eastern Canada, *Clim. Dynam.*, 6, 135–143, <https://doi.org/10.1007/BF00193525>, 1992.
- Marti, F., Blazquez, A., Meyssignac, B., Ablain, M., Barnoud, A., Fraudeau, R., Jugier, R., Chenal, J., Larnicol, G., Pfeiffer, J., Restano, M., and Benveniste, J.: Monitoring the ocean heat content change and the Earth energy imbalance from space altimetry and space gravimetry, *Earth Syst. Sci. Data*, 14, 229–249, <https://doi.org/10.5194/essd-14-229-2022>, 2022.
- McGuire, A. D., Lawrence, D. M., Koven, C., Clein, J. S., Burke, E., Chen, G., Jafarov, E., MacDougall, A. H., Marchenko, S., Nicolovsky, D., Peng, S., Rinke, A., Ciais, P., Gouttevin, I., Hayes, D. J., Ji, D., Krinner, G., Moore, J. C., Romanovsky, V., Schädel, C., Schaefer, K., Schuur, E. A. G., and Zhuang, Q.: Dependence of the evolution of carbon dynamics in the northern permafrost region on the trajectory of climate change, *P. Natl. Acad. Sci.*, 115, 3882–3887, <https://doi.org/10.1073/pnas.1719903115>, 2018.
- Melo-Aguilar, C., González-Rouco, J. F., García-Bustamante, E., Steinert, N., Jungclaus, J. H., Navarro, J., and Roldán-Gómez, P. J.: Methodological and physical biases in global to sub-continental borehole temperature reconstructions: an assessment from a pseudo-proxy perspective, *Clim. Past*, 16, 453–474, <https://doi.org/10.5194/cp-16-453-2020>, 2020.
- Neukom, R., Barboza, L. A., Erb, M. P., Shi, F., Emile-Geay, J., Evans, M. N., Franke, J., Kaufman, D. S., Lücke, L., Rehfeld, K., Schurer, A., Zhu, F., Brönnimann, S., Hakim, G. J., Henley, B. J., Ljungqvist, F. C., McKay, N., Valler, V., von Gunten, L., and the PAGES 2k Consortium: Consistent multidecadal variability in global temperature reconstructions and simulations over the Common Era, *Nature Geosci.*, 12, 643–649, <https://doi.org/10.1038/s41561-019-0400-0>, 2019.
- Nicolovsky, D. J., Romanovsky, V. E., Alexeev, V. A., and Lawrence, D. M.: Improved modeling of permafrost dynamics in a GCM land-surface scheme, *Geophys. Res. Lett.*, 34, 108501, <https://doi.org/10.1029/2007GL029525>, 2007.
- NOAA: Borehole Database at National Oceanic and Atmospheric Administration's Server, <https://www.ncdc.noaa.gov/data-access/paleoclimatology-data/datasets/borehole> (last access: September 2019), 2019.
- Oppenheimer, M., Glavovic, B., Hinkel, J., van de Wal, R., Magan, A., Abd-Elgawad, A., Cai, R., Cifuentes-Jara, M., DeConto, R., Ghosh, T., Hay, J., Isla, F., Marzeion, B., Meyssignac, B., and Sebesvari, Z.: Sea Level Rise and Implications for Low-Lying Islands, Coasts and Communities, in: IPCC Special Report on the Ocean and Cryosphere in a Changing Climate, edited by: Pörtner, H.-O., Roberts, D., Masson-Delmotte, V., Zhai, P., Tignor, M., Poloczanska, E., Mintenbeck, K., Alegría, A., Nicolai, M., Okem, A., Petzold, J., Rama, B., and Weyer, N., chap. 4, [https://www.ipcc.ch/site/assets/uploads/sites/3/2019/11/08\\_SROCC\\_Ch04\\_FINAL.pdf](https://www.ipcc.ch/site/assets/uploads/sites/3/2019/11/08_SROCC_Ch04_FINAL.pdf), 2019.
- PAGES2k Consortium: Webpage of the 2kNetwork of the Past Global Changes (PAGES) Organization, <https://pastglobalchanges.org/science/wg/2k-network/intro> (last access: 11 February 2022), 2022.
- Pendergrass, A. G. and Hartmann, D. L.: The Atmospheric Energy Constraint on Global-Mean Precipitation Change, *J. Clim.*, 27, 757–768, <https://doi.org/10.1175/JCLI-D-13-00163.1>, 2014.
- Pickler, C., Beltrami, H., and Mareschal, J.-C.: Laurentide Ice Sheet basal temperatures during the last glacial cycle as inferred from borehole data, *Clim. Past*, 12, 115–127, <https://doi.org/10.5194/cp-12-115-2016>, 2016.
- Pickler, C., Gurza Fausto, E., Beltrami, H., Mareschal, J.-C., Suárez, F., Chacon-Oecklers, A., Blin, N., Cortés Calderón, M. T., Montenegro, A., Harris, R., and Tassara, A.: Recent climate variations in Chile: constraints from borehole temperature profiles, *Clim. Past*, 14, 559–575, <https://doi.org/10.5194/cp-14-559-2018>, 2018.
- Rath, V., González Rouco, J. F., and Goosse, H.: Impact of postglacial warming on borehole reconstructions of last millennium temperatures, *Clim. Past*, 8, 1059–1066, <https://doi.org/10.5194/cp-8-1059-2012>, 2012.
- Shen, P., Wang, K., Beltrami, H., and Mareschal, J.-C.: A comparative study of inverse methods for estimating climatic history from borehole temperature data, *Global Planet. Change*, 6, 113–127, [https://doi.org/10.1016/0921-8181\(92\)90030-E](https://doi.org/10.1016/0921-8181(92)90030-E), 1992.
- Shen, P. Y., Pollack, H. N., Huang, S., and Wang, K.: Effects of subsurface heterogeneity on the inference of climate change from borehole temperature data: Model studies and field examples from Canada, *J. Geophys. Res.-Sol. Ea.*, 100, 6383–6396, <https://doi.org/10.1029/94JB03136>, 1995.
- Smerdon, J. E. and Stieglitz, M.: Simulating heat transport of harmonic temperature signals in the Earth's shallow subsurface: Lower-boundary sensitivities, *Geophys. Res. Lett.*, 33, L14402, <https://doi.org/10.1029/2006GL026816>, 2006.
- Stephens, G. L., Li, J., Wild, M., Clayson, C. A., Loeb, N., Kato, S., L'Ecuyer, T., Stackhouse, P. W., Lebsock, M., and Andrews, T.: An update on Earth's energy balance in light of the latest global observations, *Nat. Geosci.*, 5, 691–696, <https://doi.org/10.1038/ngeo1580>, 2012.
- Stevens, M. B., Smerdon, J. E., González-Rouco, J. F., Stieglitz, M., and Beltrami, H.: Effects of bottom boundary placement on subsurface heat storage: Implications for climate model simulations, *Geophys. Res. Lett.*, 34, 102702, <https://doi.org/10.1029/2006GL028546>, 2007.
- Stevens, M. B., González-Rouco, J. F., and Beltrami, H.: North American climate of the last millennium: Underground temperatures and model comparison, *J. Geophys. Res.-Ea. Surf.*, 113, f01008, <https://doi.org/10.1029/2006JF000705>, 2008.
- Suman, A., Dyer, F., and White, D.: Late Holocene temperature variability in Tasmania inferred from borehole temperature data, *Clim. Past*, 13, 559–572, <https://doi.org/10.5194/cp-13-559-2017>, 2017.
- Turcotte, D. L. and Schubert, G.: *Geodynamics*, Cambridge University Press, 2nd edition edn., 2002.
- Vanderkelen, I., van Lipzig, N. P. M., Lawrence, D. M., Dropers, B., Golub, M., Gosling, S. N., Janssen, A. B. G., Marcé, R., Schmied, H. M., Perroud, M., Pierson, D., Pokhrel, Y., Satoh, Y., Schewe, J., Seneviratne, S. I., Stepanenko, V. M., Tan, Z., Woolway, R. I., and Thiery, W.: Global Heat Uptake by Inland Waters, *Geophys. Res. Lett.*, 47, e2020GL087867, <https://doi.org/10.1029/2020GL087867>, 2020.
- Vasseur, G., Bernard, P., de Meulebrouck, J. V., Kast, Y., and Jolivet, J.: Holocene paleotemperatures deduced from geothermal mea-

- surements, *Palaeogeogr. Palaeoclimatol. Palaeoecol.*, 43, 237–259, [https://doi.org/10.1016/0031-0182\(83\)90013-5](https://doi.org/10.1016/0031-0182(83)90013-5), 1983.
- von Schuckmann, K., Cheng, L., Palmer, M. D., Hansen, J., Tassone, C., Aich, V., Adusumilli, S., Beltrami, H., Boyer, T., Cuesta-Valero, F. J., Desbruyères, D., Domingues, C., García-García, A., Gentile, P., Gilson, J., Gorfer, M., Haimberger, L., Ishii, M., Johnson, G. C., Killick, R., King, B. A., Kirchengast, G., Kolodziejczyk, N., Lyman, J., Marzeion, B., Mayer, M., Monier, M., Monselesan, D. P., Purkey, S., Roemmich, D., Schweiger, A., Seneviratne, S. I., Shepherd, A., Slater, D. A., Steiner, A. K., Straneo, F., Timmermans, M.-L., and Wijffels, S. E.: Heat stored in the Earth system: where does the energy go?, *Earth Syst. Sci. Data*, 12, 2013–2041, <https://doi.org/10.5194/essd-12-2013-2020>, 2020.
- Wang, J. and Bras, R.: Ground heat flux estimated from surface soil temperature, *J. Hydrol.*, 216, 214–226, [https://doi.org/10.1016/S0022-1694\(99\)00008-6](https://doi.org/10.1016/S0022-1694(99)00008-6), 1999.
- Woodbury, A. D. and Ferguson, G.: Ground surface paleotemperature reconstruction using information measures and empirical Bayes, *Geophys. Res. Lett.*, 33, L06702, <https://doi.org/10.1029/2005GL025243>, 2006.